

1                   **Nonlinear ENSO Warming Suppression (NEWS)**

2                   **causing a La Niña-like mean-state response to global warming**

3                   Tsubasa Kohyama\* and Dennis L. Hartmann

4                   *Department of Atmospheric Sciences, University of Washington, Seattle, Washington*

5 \**Corresponding author address:* Department of Atmospheric Sciences, University of Washington,

6 Box 351640, Seattle, WA 98195-1640

7 E-mail: kohyama@uw.edu

## ABSTRACT

8 In global warming experiments, the majority of global climate models warm  
9 faster in the eastern equatorial Pacific than in the west and produce a weaken-  
10 ing of the Walker circulation. Recently, however, Kohyama, Hartmann, and  
11 Battisti (2016) showed that GFDL-ESM2M is an exception that exhibits a La  
12 Niña-like mean-state warming with a strengthening of the Walker circulation.  
13 This study explores the cause of this exceptional response and proposes a new  
14 mechanism, the Nonlinear ENSO Warming Suppression (NEWS), where the  
15 transient heating rate difference between the atmospheric and oceanic reser-  
16 voirs annihilates extreme El Niños, causing a suppression of the mean-state  
17 warming in the east. Heat budget analyses of GFDL-ESM2M robustly show  
18 that nonlinear dynamical heating, which is necessary for extremely warm El  
19 Niños, becomes negligible under warming. An idealized nonlinear recharge  
20 oscillator model suggests that, if the temperature difference between the at-  
21 mospheric and oceanic reservoirs becomes larger than some threshold value,  
22 the upwelling becomes too efficient for the El Niño Southern Oscillation  
23 (ENSO) to keep its nonlinearity. Therefore, extreme El Niños dissipate but La  
24 Niñas remain almost unchanged, causing a La Niña-like mean-state warming.  
25 NEWS is consistent with observations and GFDL-ESM2M but not with the  
26 majority of state-of-the-art models, which lack realistic ENSO nonlinearity.  
27 NEWS and its opposite response to atmospheric cooling might contribute to  
28 the Pacific multi-decadal natural variability and global warming hiatuses.

## 29 **1. Introduction**

30 The tropical Pacific Ocean is one of the main contributors to variability in the Earth's climate  
31 system, but whether the mean-state sea surface temperature (SST) response of this region to global  
32 warming should be "El Niño-like" (SST warms faster in the east) or "La Niña-like" (SST warms  
33 faster in the west) is uncertain from the perspective of observations (Rayner et al. 2003; Smith  
34 et al. 2008; Christensen et al. 2013), models (Knutson and Manabe 1995; Cane et al. 1997; Vecchi  
35 and Soden 2007), and theory (Clement et al. 1996; Collins et al. 2005, 2010; Xie et al. 2010; Held  
36 et al. 2010; An et al. 2012). In this study we use the terms "El Niño-like" and "La Niña-like" due  
37 to their lucidity and simplicity, it is controversial whether it is appropriate to use them to describe  
38 the tropical SST response to warming. This controversy is because these terms are associated  
39 with the El Niño Southern Oscillation (ENSO), a dominant interannual natural climate mode that  
40 modulates the SST deviations from the tropical Pacific mean state, which may not necessarily be  
41 similar to a forced global warming response (Collins et al. 2010). In global warming projections,  
42 however, it is extremely important to understand possible processes that determine the mean-state  
43 changes in this region and to narrow their major uncertainties, because the tropical Pacific mean-  
44 state variability and its changes are expected to have substantial scientific and societal impacts on  
45 not only the tropics and subtropics (e.g., droughts, floods, heat waves, poor harvests, changing  
46 marine ecosystems) but also the mid-latitudes and high-latitudes (e.g., cold spells, changing trop-  
47 ical cyclone genesis frequency, modulating Antarctic sea ice trends) (Yokoi and Takayabu 2009;  
48 Christensen et al. 2013; Kohyama and Hartmann 2016).

49 The vast majority of the state-of-the-art global climate models (GCM) that participated in the  
50 Coupled Model Intercomparison Project Phase 5 (CMIP5) exhibit El Niño-like mean-state re-  
51 sponses to global warming. These responses are widely believed to be associated with a weak-

52 ening of the Walker Circulation, which some believe is necessary to sustain a global-mean wa-  
53 ter and energy balance derived by (Held and Soden 2006). This necessity was supported by  
54 the multi-model mean behavior of CMIP3 models as shown by Vecchi and Soden (2007). A  
55 recent work by Kohyama, Hartmann, and Battisti (2016) (hereafter KHB16; in review, avail-  
56 able at [http://www.atmos.washington.edu/~kohyama/papers/KHB16\\_lanina\\_ver5.pdf](http://www.atmos.washington.edu/~kohyama/papers/KHB16_lanina_ver5.pdf)),  
57 however, showed that GFDL-ESM2M (a GCM developed by Geophysical Fluid Dynamics Lab-  
58 oratory) is an interesting exception in that it produces a well-defined La Niña-like mean-state  
59 warming with a clear strengthening of the Walker circulation. They also showed that its telecon-  
60 nection patterns in extratropical temperatures and precipitation are also different from those of  
61 a model that exhibits an El Niño-like mean-state SST change similar to the multi-model mean  
62 response.

63 In particular, a remarkable structural resemblance of the strengthening Walker circulation be-  
64 tween the GFDL-ESM2M and observations during the satellite era increases the interest in in-  
65 vestigating this model further to determine whether this observed change is purely due to natural  
66 multi-decadal variability or partly a forced response to global warming. One might be concerned  
67 that this strengthening Walker circulation could violate the robust energy and water balance pro-  
68 posed by Held and Soden (2006). KHB16 showed that, however, the balance only constrains the  
69 global-mean change, but not necessarily a regional response (e.g., the Walker circulation), so it is  
70 still possible to simulate a strengthening Walker circulation if a more dominant, opposite forcing  
71 exists. Comparing with the GFDL-ESM2G, which differs from the GFDL-ESM2M only by its  
72 oceanic component, KHB16 suggested that an important oceanic mechanism might play a ma-  
73 jor role in controlling the mean-state SST warming response, which then forces the atmospheric  
74 circulation changes.

75 KHB16 also concluded that, in the GFDL-ESM2M, the observed correlation between the zonal  
76 SST gradient and the amplitude of ENSO is particularly well-reproduced, and that its La Niña-like  
77 mean-state warming trend in response to warming may be causally related to the weakening ENSO  
78 amplitude. This hypothetical relationship is also consistent with a recent paper by Zheng et al.  
79 (2016), which showed that a group of four CMIP5 models with a La Niña-like warming shows a  
80 weakening of the ENSO amplitude. Therefore, we would like to understand why the ENSO in this  
81 particular model is weakened under a warmer climate. The top panels of Fig. 1 show the SST  
82 during December-January-February (DJF) averaged over the western equatorial warm pool region  
83 ( $5^{\circ}\text{N}$ - $5^{\circ}\text{S}$ ,  $130^{\circ}\text{E}$ - $160^{\circ}\text{E}$ ) and the eastern equatorial cold tongue ( $5^{\circ}\text{N}$ - $5^{\circ}\text{S}$ ,  $120^{\circ}\text{W}$ - $90^{\circ}\text{W}$ ), as in the  
84 Fig. 1 of An and Jin (2004) (hereafter AJ04) but for the preindustrial control (piControl) and abrupt  
85 quadrupling carbon dioxide ( $\text{CO}_2$ ) (Abrupt4x $\text{CO}_2$ ) runs defined by the CMIP5 project. Only the  
86 years after Year 100 are shown for the Abrupt4x $\text{CO}_2$  run, because it takes a couple of decades  
87 before the climate reaches its quasi-equilibrium after the abrupt  $\text{CO}_2$  increase (not shown). The  
88 ENSO amplitude is substantially suppressed in a warmer climate in the GFDL-ESM2M, which is  
89 consistent with the result shown in KHB16 based on the Representative Concentration Pathway  
90 (RCP) 8.5 run.

91 More importantly, the SST time series of Abrupt4x $\text{CO}_2$  show no extreme El Niño (EEN) events.  
92 Here, we refer to El Niño events as EENs if the cold tongue SST closely approaches or surpasses  
93 the warm pool SST. In the observed record, the El Niños in 1982/83 and 1997/98 are classified as  
94 EENs as we will show later in this section. Jin et al. (2003) and AJ04 called the western warm pool  
95 SST “the upper bound” of the eastern cold tongue SST, defining this upper bound as the maximum  
96 potential intensity (MPI) of an El Niño as a theoretical measure. One of the main conclusions  
97 of Jin et al. (2003) and AJ04 was that, during EENs, the climatological conditions of the ocean  
98 and atmosphere are completely collapsed and that one cannot treat EENs as linear perturbations

99 from the climatological mean. In Fig. 2, we have reproduced some figures shown in AJ04 but  
 100 with a longer record. The SST spatial pattern during the EEN in 1997/98 DJF shows a completely  
 101 different structure than the climatological SST. Moreover, the equatorial upper ocean temperature  
 102 clearly shows that, during the EEN, the thermocline is almost flat across the equatorial Pacific.  
 103 This is virtually the largest El Niño that can potentially occur, which is why AJ04 defined the  
 104 warm pool SST as the MPI. The eastern equatorial SST is bounded by the MPI, and the MPI is, in  
 105 turn, determined by the radiative-convective equilibrium temperature (Waliser and Graham 1993).

106 The next question, then, is whether the mechanisms that cause EENs and normal ENSO events  
 107 are different. Jin et al. (2003) and AJ04 addressed this question by performing a heat budget  
 108 analysis of the upper ocean by decomposing the dynamical heating terms into “Linear Dynamical  
 109 Heating (LDH)” and “Nonlinear Dynamical Heating (NDH)”. The heat budget of the mixed layer  
 110 can be written in the form of the following equation:

$$\frac{\partial T'}{\partial t} = \left( -u' \frac{\partial \bar{T}}{\partial x} - v' \frac{\partial \bar{T}}{\partial y} - w' \frac{\partial \bar{T}}{\partial z} - \bar{u} \frac{\partial T'}{\partial x} - \bar{v} \frac{\partial T'}{\partial y} - \bar{w} \frac{\partial T'}{\partial z} \right) + \left( -u' \frac{\partial T'}{\partial x} - v' \frac{\partial T'}{\partial y} - w' \frac{\partial T'}{\partial z} \right) + R' \quad (1)$$

111 where  $t$  denotes time,  $x$ ,  $y$ , and  $z$  denote the zonal, meridional, and vertical coordinates, respec-  
 112 tively, and  $T$ ,  $u$ ,  $v$ , and  $w$  are mixed layer temperature, eastward, northward, and upward velocities,  
 113 respectively. Overlines denote the monthly climatological mean, and primes denote the deviations  
 114 therefrom. Surface heat flux and subgrid-scale contributions are all included in the residual term  
 115  $R$ . AJ04 defined the terms in the first (second) bracket as LDH (NDH).

116 Most important among the NDH terms is the vertical component. During El Niño events, anoma-  
 117 lous downwelling tends to occur simultaneously with anomalously strong stratification; therefore,  
 118 NDH warms the mixed layer. During La Niña events, however, anomalous upwelling occurs with  
 119 anomalously weak stratification. In other words, the upwelling advects anomalously warm water

120 from the bottom, so NDH again warms the mixed layer. Mathematically, the covariance between  
121 downwelling ( $-w'$ ) and the temperature gradient ( $\partial T'/\partial z$ ) remains positive in both El Niños and  
122 La Niñas. Hence, the resulting total dynamical heating flux (LDH+NDH) warms the surface a lot  
123 in El Niño events but cools the surface a little in La Niña events. This asymmetry is why large El  
124 Niños (including EENs) are observed, but not as large La Niñas as them. Furthermore, as seen in  
125 the time series of MPI, the cold tongue SST, NDH and LDH calculated for the uppermost 50m in  
126 Fig. 2 (c), LDH is always important, but NDH is comparable to LDH only for EENS (i.e., 1982/83  
127 and 1997/98). It is also suggestive that NDH contribution is almost negligible after 1999. Inter-  
128 estingly, at least by this metric, the recent large El Niño in 2015/16 may not be classified an EEN,  
129 which is consistent with the fact that the El Niño in 2015/16 was the largest in historical record in  
130 terms of the Niño 3.4 index (SST averaged over  $5^{\circ}\text{N}$ - $5^{\circ}\text{S}$ ,  $170^{\circ}\text{W}$ - $120^{\circ}\text{W}$ ) but not in terms of the  
131 Niño 3 index ( $5^{\circ}\text{N}$ - $5^{\circ}\text{S}$ ,  $170^{\circ}\text{W}$ - $120^{\circ}\text{W}$ ) (not shown).

132 Based on this observational evidence shown by AJ04, we hypothesize that, at least in the GFDL-  
133 ESM2M, the reason why EENs are not detected in Abrupt4xCO<sub>2</sub> may be that NDH becomes  
134 unimportant in a warmer climate. The middle and bottom panels in Fig. 1 show the time series  
135 of NDH and LDH for the upper 50 m, respectively, in both piControl and Abrupt4xCO<sub>2</sub>. As  
136 expected, the NDH becomes much weaker in the warmer run, whereas LDH remains stationary to  
137 first order. This dominance of LDH means that ENSO in a warmer climate becomes almost linear,  
138 and the dissipation of NDH is a main contributor to the weakening ENSO amplitude in this model.

139 Hence, the questions we address in this paper are as follows: (i) Why does NDH become unim-  
140 portant in a warmer climate in the GFDL-ESM2M? (And, as a corollary, can we expect that fewer  
141 EENs will be observed in the future?) (ii) Can the weakening of ENSO amplitude due to the weak-  
142 ening of NDH cool the mean-state SST of the cold tongue? (iii) Is the weakening ENSO amplitude  
143 a cause or an effect of the La Nina-like mean state warming in the GFDL-ESM2M (or neither)?

144 (iv) Why does the GFDL-ESM2M simulate these processes but other models do not? (What are  
145 the necessary conditions for simulating those processes? Are those processes realistic?) (v) Do  
146 these mechanisms also have implications for multi-decadal natural variability? Despite some risk  
147 in exploring processes simulated by only a minority of models, we would like to understand why  
148 GFDL-ESM2M can be the minority in such a major property of GCMs. Considering its challenge  
149 as a scientific problem and its societal impact, the outcome is so important that we believe we must  
150 understand this inter-model difference better.

151 This article is organized as follows. The data and an idealized model used in this study are  
152 described in the next section. In section 3, the idealized model is used to explore why NDH be-  
153 comes negligible in a warmer climate; furthermore, we confirm that these ideas are consistent with  
154 GFDL-ESM2M output. Then, in section 4, we further compare the idealized model, observations,  
155 and GFDL-ESM2M output to propose a mean-state warming suppression mechanism as a forced  
156 response of the cold tongue to global warming. We also discuss the reason why only the GFDL-  
157 ESM2M can simulate this mechanism, as well as the important difference between gradual and  
158 abrupt CO<sub>2</sub> increases. In section 5, we explore some implications of the above mechanism for  
159 multi-decadal natural variability and global warming hiatuses. Conclusions are given in section 6.

## 160 **2. Data and an Idealized Model**

### 161 *a. Data*

162 Observed monthly SSTs are from the Hadley Centre Sea Ice and Sea Surface Temperature  
163 (HadISST) (Rayner et al. 2003) available online at [http://www.metoffice.gov.uk/hadobs/  
164 hadisst/index.html](http://www.metoffice.gov.uk/hadobs/hadisst/index.html) for the period 1880 through 2015. Except for Fig. 11, we use SST data  
165 from the period 1965 through 2015, during which we expect the data to be less influenced by

166 limited data sampling, changing measurement techniques, and analysis procedure dependence  
167 (Christensen et al. 2013). Whenever we show time series, we add the data of the first half of  
168 2016 so that we do not miss the 2015/16 El Niño. The spatial resolution is 1° latitude by 1°  
169 longitude. Reanalyzed oceanic potential temperature and horizontal velocity data are obtained  
170 from the National Centers for Environmental Prediction (NCEP) Global Ocean Data Assimilation  
171 System (GODAS) (Behringer and Xue 2004) available online at [http://www.esrl.noaa.gov/  
172 psd/data/gridded/data.godas.html](http://www.esrl.noaa.gov/psd/data/gridded/data.godas.html). The horizontal resolution is 1° longitude by 1/3° lat-  
173 itude, with a vertical resolution of 10 m for uppermost 230 m (no data deeper than 230m are  
174 used in this study). The oceanic vertical motion at 50 m depth is calculated assuming mass  
175 continuity with negligible density tendency, which exhibits very good agreement with vertical  
176 motion data available at the NCEP GODAS website. This agreement confirms the validity of  
177 this assumption and the algorithms we use for the model output described in the next paragraph.  
178 Finally, annual-mean, global-mean observed surface temperature is downloaded from the God-  
179 dard Institute for Space Studies (GISS) Surface Temperature Analysis (GISTEMP) (Hansen et al.  
180 2010) produced by GISTEMP Team 2016 at the National Aeronautics and Space Administra-  
181 tion (NASA) Goddard Institute for Space Studies. The data was accessed on 2016-07-07 at  
182 <http://data.giss.nasa.gov/gistemp/>, to make Fig. 11.

183 The surface temperature, oceanic potential temperature, and horizontal velocity output from  
184 the GFDL-ESM2M are taken from the GFDL Data Portal ([http://nomads.gfdl.noaa.gov:  
185 8080/DataPortal/cmip5.jsp](http://nomads.gfdl.noaa.gov:8080/DataPortal/cmip5.jsp)). The experiments considered in this study are the first ensem-  
186 ble member of the piControl, Abrupt4xCO<sub>2</sub>, 1% per year increase in CO<sub>2</sub> (1pctCO<sub>2</sub>), RCP  
187 6.0, and RCP 8.5 runs. At each depth, the oceanic variables are regridded via linear interpo-  
188 lation onto a 2.5° longitude by 2° latitude grid; the oceanic data have a vertical resolution of  
189 10 m for the uppermost 230 m. The oceanic vertical motion at 50 m depth is calculated us-

190 ing the same procedure as described above. We also use other CMIP5 (Taylor et al. 2012)  
191 model output available at the Program for Climate Model Diagnosis and Intercomparison web-  
192 site (<https://pcmdi.llnl.gov/projects/cmip5/>) for making Fig. 7.

193 Using the aforementioned oceanic data, LDH and NDH of the mixed layer are calculated using  
194 the equation (1) at each gridpoint, assuming that the mixed layer depth is fixed at 50 m. As in  
195 AJ04, we have confirmed that the results shown in this paper are not sensitive to the choice of  
196 the mixed layer depth and its variability. To calculate LDH and NDH, the monthly climatology  
197 ( $\bar{T}$ ,  $\bar{u}$ ,  $\bar{v}$ , and  $\bar{w}$ ) is calculated as the mean over the entire record for each month, except that linear  
198 trends are also added in RCP8.5, because the mean-state climatology also warms in this run. The  
199 LDH and NDH time series are calculated as the regional average over 5°N-5°S, 170°W-100°W,  
200 following AJ04. The oceanic reservoir temperature beneath the thermocline ( $T_o$ ) is calculated as  
201 the temperature at 100m below the thermocline (the thermocline depth is defined as the depth with  
202 the maximum vertical temperature gradient). The results are not sensitive to this choice of depth  
203 (i.e., 100m), unless it is too close to the thermocline where the temperature has a larger interannual  
204 variance.

### 205 *b. Idealized Model*

206 We use an idealized nonlinear recharge oscillator model introduced by Jin (1998) and Timmer-  
207 mann et al. (2003) and its modified versions. This model is essentially a simplified, two-box  
208 approximation of the Cane-Zebiak model (Zebiak and Cane 1987). The tendency of the tempera-  
209 ture of the oceanic mixed layer in the western warm pool ( $T_1$ ) and the eastern cold tongue ( $T_2$ ) are  
210 :

$$\frac{dT_1}{dt} = -\alpha(T_1 - T_a) - \frac{u}{L/2}(T_2 - T_1) \quad (2)$$

211

$$\frac{dT_2}{dt} = -\alpha(T_2 - T_a) - \frac{w}{H_m}(T_2 - T_{\text{sub}}) \quad (3)$$

212

213

214

215

216

where  $1/\alpha$  denotes a thermal damping time scale,  $T_{\text{sub}}$  denotes subsurface temperature, and  $u$  and  $w$  are eastward and upward oceanic velocities, respectively.  $H_m$  and  $L$  are the mixed layer depth and the basin width, respectively.  $T_a$  denotes the zonally uniform lower atmospheric reservoir temperature, but except for section 5,  $T_a$  is replaced by the radiative-convective equilibrium temperature  $T_r$  as in Jin (1998) and Timmermann et al. (2003):

$$T_a = T_r \quad (4)$$

217

218

219

Both  $T_1$  and  $T_2$  are relaxed toward  $T_a$  by the first terms of the equations (2) and (3), and the second terms of (2) and (3) express the zonal and vertical temperature advection, respectively. Then, the wind stress  $\tau$ ,  $u$ , and,  $w$  are expressed as:

$$\tau = -\mu(T_1 - T_2)/\beta \quad (5)$$

220

$$\frac{u}{L/2} = \varepsilon\beta\tau \quad (6)$$

221

$$\frac{w}{H_m} = -\zeta\beta\tau \quad (7)$$

222

223

224

where  $\mu$  is the sensitivity of the trade wind to the zonal SST gradient, and  $\varepsilon$  and  $\zeta$  are zonal advection and upwelling efficiency (i.e., sensitivities of zonal and vertical oceanic currents to the trade wind), respectively. Parameterization of  $T_{\text{sub}}$  is given by Jin (1996) as:

$$T_{\text{sub}} = T_a - \frac{T_a - T_o}{2} \left( 1 - \tanh \frac{H + h_2 - z_0}{h^*} \right) \quad (8)$$

225

226

227

where  $T_o$  is the oceanic reservoir temperature beneath the thermocline,  $h_2$  is the departure of the eastern thermocline depth from the reference depth  $H$ ,  $z_0$  is the depth at which  $w$  takes its characteristic values, and  $h^*$  is a scale parameter that controls the sharpness of the thermocline.

228 The thermocline depth departure  $h_1$  (west) and  $h_2$  (east) follow the recharge oscillator (Jin 1997)  
 229 formulations:

$$\frac{dh_1}{dt} = -rh_1 - \left(\frac{rbL}{2}\right) \tau \quad (9)$$

$$h_2 = h_1 + bL\tau \quad (10)$$

231 where  $1/r$  denotes the damping time scale of the anomaly, and  $b$  is the sensitivity of the thermo-  
 232 cline to the trade wind change due to the Sverdrup transport. The parameter values used in this  
 233 study follow AJ04 ( $\alpha = 1/180 \text{ day}^{-1}$ ,  $r = 1/400 \text{ day}^{-1}$ ,  $H_m = 50 \text{ m}$ ,  $H = 100 \text{ m}$ ,  $z_0 = 75 \text{ m}$ ,  
 234  $h^* = 62 \text{ m}$ ,  $\mu = 0.0026 \text{ K}^{-1} \text{ day}^{-1}$ ,  $\mu bL/\beta = 22 \text{ m K}^{-1}$ ,  $\zeta = 1.3$ ,  $\varepsilon = 0.11$ , and  $L = 15 \times 10^6 \text{ m}$ )  
 235 except for some modifications described below.

236 Timmermann et al. (2003) and AJ04 introduced  $T_r$  ( $T_a$ ) and  $T_o$  as constant parameters equaling  
 237  $29.5 \text{ }^\circ\text{C}$  and  $16 \text{ }^\circ\text{C}$ , respectively. Here, to simulate the change of the radiative-convective equilib-  
 238 rium temperature and the reservoir temperature associated with global warming, we modify  $T_r$  and  
 239  $T_o$  to be simple linear functions of time:

$$\frac{dT_r}{dt} = Q_r, \quad \text{or} \quad T_r = Q_r t + T_C \quad (11)$$

$$\frac{dT_o}{dt} = Q_o, \quad \text{or} \quad T_o = Q_o t + T_D \quad (12)$$

241 where  $Q_r$ ,  $Q_o$ ,  $T_C$ , and  $T_D$  are test parameters that we will vary in the following sections. One  
 242 of the main ideas presented in this paper is that  $T_a - T_o$  ( $= T_r - T_o$  except for section 5) is a key  
 243 parameter that determines the prominence of NDH and EENs. In “fixed reservoir temperature  
 244 difference” experiments, we set  $Q_r = Q_o = 0$ , and in “increasing reservoir temperature difference”  
 245 experiments, we set  $Q_r > Q_o > 0$ .

246 In section 5, we further generalize the idealized model, particularly equation (4), so that  $T_a$   
 247 becomes capable of responding to the eastern equatorial mean-state multi-decadal variability. As  
 248 shown in Kosaka and Xie (2013) and many others, a La Niña-like mean climate generally enhances

249 the atmospheric cooling by the eastern equatorial Pacific, leading to global warming hiatuses or  
 250 slowdowns. An El Niño-like mean-state, on the other hand, suppresses the atmospheric cooling  
 251 rate. Therefore, the tendency of  $T_a$  and its heating rate  $R_a$  are expressed as the following equations:

$$\frac{dT_a}{dt} = R_a \quad (13)$$

$$\frac{dR_a}{dt} = -\omega^2(T_a - T_r) - \gamma(T_a - T_2) \quad (14)$$

252  
 253 where  $\gamma$  denotes the sensitivity of atmospheric heating rate to the cold tongue SST, and  $\omega$  is a  
 254 normal-mode angular frequency of generalized multi-decadal atmospheric natural variability that  
 255 restores the atmospheric temperature toward radiative-convective equilibrium. This natural vari-  
 256 ability could be a synthesized effect of, for instance, the Planck feedback, water vapor feedback,  
 257 ice-albedo feedback, cloud feedback, and so on. Therefore, the restoring effect expressed as the  
 258 first term in the equation (14) is not a simple relaxation that involves only negative feedbacks;  
 259 rather, it excites an oscillatory behavior that involves both positive and negative feedbacks. The  
 260 second term expresses a forcing by the eastern equatorial Pacific that cools the atmosphere, and  
 261 we try to understand the atmospheric temperature variability as a forced oscillation. In this con-  
 262 figuration, we could interpret the equation (4) as a limit of infinitesimal atmospheric sensitivity to  
 263 the Pacific cold tongue ( $\gamma = 0$ ) and infinitesimally low frequency of the atmospheric normal mode  
 264 ( $\omega = 0$ ) with initial conditions of  $T_a(t = 0) = T_c$  and  $R_a(t = 0) = Q_r$ . The parameter values are  
 265 tuned to  $\gamma = 0$  (zero sensitivity experiments) or  $2 \times 10^{-9} \text{ day}^{-2}$  (i.e.,  $1/13700 \text{ year}^{-2}$ ) (non-zero  
 266 sensitivity experiments) and  $\omega = 2\pi/90 \text{ rad year}^{-1}$  so that the model realistically simulates the  
 267 phenomena of interest.

268 Following Timmermann et al. (2003), the above idealized model is integrated forward in time  
 269 using a Runge-Kutta method of fourth order with a time step of 1 day. The results presented  
 270 in section 3 and 4 are not sensitive to initial conditions if realistic initial conditions are chosen.

271 In section 5, however, because of the more complicated model configuration, the range of initial  
272 conditions that reproduce our results appears to be narrower. In our study, we have used the initial  
273 conditions of  $T_1 = 27$  °C,  $T_2 = 20$  °C,  $h_1 = 70$  m,  $T_a = T_r = 29.5$  °C,  $T_o = 15$  °C, and  $R_a = 0$   
274 °C/century at  $t = 0$ .

### 275 **3. Dissipation of nonlinear dynamical heating (NDH) and extreme El Niño (EEN) events due** 276 **to an increasing temperature difference between the atmospheric and oceanic reservoirs**

277 In this section, we first use the idealized nonlinear recharge oscillator model to obtain some  
278 ideas for why the NDH becomes unimportant in warmer runs of the GFDL-ESM2M. Then, we  
279 further analyze the output from the GFDL-ESM2M to show that the idealized model captures the  
280 behavior of the GFDL-ESM2M reasonably well.

#### 281 *a. Key parameter $T_a - T_o$*

282 Figure 3 (a) shows MPI (i.e., warm pool SST,  $T_1$ ), the cold tongue SST ( $T_2$ ), and the NDH  
283 time series simulated by the idealized model with fixed reservoir temperature difference  $T_a -$   
284  $T_o = 12.0$  °C,  $13.9$  °C,  $14.1$  °C, and  $14.3$  °C. Here we fix  $T_a = 29.5$  °C and vary  $T_o$  to realize  
285 different values of  $T_a - T_o$ , but we obtain nearly identical results if we fix  $T_o$  and change  $T_a$  instead.  
286 As Timmermann et al. (2003) showed by changing either the zonal advection ( $\epsilon$ ) or upwelling  
287 efficiency ( $\zeta$ ), some different regimes of the ENSO variability are identifiable. The regime with  
288  $T_a - T_o = 12.0$  °C corresponds to a regime with a strong zonal advection, where all ENSO events are  
289 EENs (i.e., the cold tongue SST always reaches the MPI). As  $T_a - T_o$  becomes larger ( $T_a - T_o = 13.9$   
290 °C), the frequency of EENs decreases with lengthening, intermittent linear periods in between  
291 EENs, whose basic dynamics can be explained by the linear recharge oscillator system. Then, the  
292 intervals between EENs become longer and irregular at  $T_a - T_o = 14.1$  °C, and the EENs finally

293 vanish at the  $T_a - T_o = 14.3$  °C regime. In this last regime, the ENSO becomes completely linear  
 294 and no EENs are detected. These four experiments are consistent with observations that the NDH  
 295 is only important for EENs as shown in Fig. 2 (c) and by AJ04.

296 Based on the results obtained from the “fixed reservoir temperature difference” runs, we surmise  
 297 that a “threshold reservoir temperature difference” at which the importance of NDH bifurcates ex-  
 298 ists between 14.1 °C and 14.3 °C. To test this idea, we have performed an “increasing reservoir  
 299 temperature difference” run, where we gradually increase the  $T_a - T_o$  linearly in time. As an ana-  
 300 logue for global warming, we have simulated the increasing temperature difference by setting dif-  
 301 ferent heating rates,  $Q_r = 1$  °C/century and  $Q_o = 0.3$  °C/century, for the atmospheric and oceanic  
 302 reservoirs. Figure 3 (b) shows the result of this run, and, as expected, the intervals between the  
 303 EENs become gradually longer (from about 12 to 18 year intervals) as the system warms, and the  
 304 system exhibits no EENs and NDH after  $T_a - T_o$  surpasses 14.2 °C in Year 100.

305 Mathematically, it is easy enough to understand why the system exhibits the same regime shift  
 306 as the one shown in Timmermann et al. (2003). In their Fig 6, for a given efficiency of zonal  
 307 advection ( $\epsilon$ ), they varied the efficiency of upwelling ( $\zeta$ ) with  $T_a$  and  $T_o$  fixed, whereas we have  
 308 varied  $T_a - T_o$  with  $\zeta$  fixed. It turns out that varying  $T_a - T_o$  yields essentially the same effect as  
 309 changing the upwelling efficiency  $\zeta$ . Because variations of  $T_a - T_o$  only influence equation (8), the  
 310 increase of  $T_a - T_o$  means a decrease of  $T_{\text{sub}}$ , or an increase  $(T_2 - T_{\text{sub}})/H_m$  (vertical temperature  
 311 gradient) in the equation (3). Because  $(T_2 - T_{\text{sub}})/H_m$  is multiplied by  $w = -\zeta\beta\tau H_m$  in equation  
 312 (3), it is evident that increased  $T_a - T_o$  has the same effect on the tendency of  $T_2$  as increased  $\zeta$ .

313 Physically, the above mathematical explanation can be translated as follows. If global warm-  
 314 ing heats the lower atmosphere faster than the ocean interior beneath the thermocline, it tends  
 315 to enhance the upper ocean stratification, which in turn enhances the mixed-layer cooling by the  
 316 equatorial upwelling. Hence, this overwhelming upwelling prevents the thermocline from recharg-

317 ing the heat enough to collapse its climatological mean structure. This means a complete damping  
318 of NDH, making it difficult for a warm SST anomaly to mature in response to westerly wind  
319 anomalies.

320 *b. Comparison with GFDL-ESM2M*

321 In state-of-the-art GCMs and in the real world, the lower atmospheric temperature should warm  
322 faster than the ocean interior beneath the thermocline, because of the large oceanic heat capacity  
323 and the slow oceanic circulation compared to the atmospheric counterparts. Therefore, as a tran-  
324 sient response to global warming,  $T_a - T_o$  should become larger as the Earth warms, and this may  
325 be why no NDH and EENs are detected in a warmer climate in the GFDL-ESM2M. To test this  
326 hypothesis, we have calculated the time series of  $T_a - T_o$  in the GFDL-ESM2M using the warm  
327 pool SST as a proxy for  $T_a$  (because, in section 3,  $T_a$  is equal to the radiative-convective equi-  
328 librium temperature) and the temperature 100 m below the thermocline, averaged over the cold  
329 tongue region ( $5^\circ\text{S}$ - $5^\circ\text{N}$  and  $120^\circ\text{W}$ - $90^\circ\text{W}$ ), as a proxy for  $T_o$  (see also section 2).

330 Figure 4 shows the time series of MPI, the cold tongue SST, NDH, and  $T_a - T_o$  for the piControl,  
331 RCP8.5, and Abrupt4xCO<sub>2</sub> runs of GFDL-ESM2M. As already pointed out in Fig. 1, GFDL-  
332 ESM2M occasionally exhibits EENs and NDH in piControl (nonlinear regime), but no EENs and  
333 NDH in Abrupt4xCO<sub>2</sub> (linear regime). In accordance with a gradual warming in RCP 8.5, the  
334 model exhibits a clear transition from the nonlinear regime to the linear regime. More impor-  
335 tantly, our key parameter  $T_a - T_o$  also increases by about  $1^\circ\text{C}$  as the regime shifts, suggesting that  
336 the ideas obtained from the idealized model experiments are consistent with the behavior of the  
337 GFDL-ESM2M.

338 To further confirm the consistency between the idealized model and GFDL-ESM2M, in Fig.  
339 5, we have also plotted phase diagrams showing the relationship between the cold tongue SST

340 anomalies and western thermocline depth departure anomalies. The phase diagrams of both mod-  
341 els exhibit a reasonable resemblance with each other, and the mechanism can be explained as  
342 follows. In the nonlinear regime with low upwelling efficiency, the Sverdrup transport caused by  
343 the trade wind recharges the heat in the equatorial mixed layer and the thermocline depth grad-  
344 ually becomes deeper than the norm, which in turn causes inefficient upwelling, and finally, an  
345 extremely warm SST anomaly in the cold tongue (i.e., EEN). In the linear regime with high up-  
346 welling efficiency, however, the trade wind cannot recharge the heat in the mixed layer because of  
347 the stronger upwelling cooling, so the thermocline cannot become deep enough to excite an event  
348 with a huge SST anomaly in the east.

#### 349 **4. Nonlinear ENSO Warming Suppression (NEWS)**

350 In this section, we further compare the idealized model with observations and GFDL-ESM2M  
351 output to show that the forced, nonlinear EEN dissipation due to the transient increase of  $T_a - T_o$   
352 has a warming suppression effect on the mean state of the eastern equatorial Pacific SST. We also  
353 explore some necessary conditions to simulate this mechanism by comparing GFDL-ESM2M to  
354 other models. Furthermore, we focus on the different mean-state responses between gradual and  
355 abrupt warming runs to emphasize the transient feature of this mechanism and to determine the  
356 direction of causality between the ENSO amplitude change and the mean-state change.

##### 357 *a. NEWS as a forced response to global warming*

358 In the previous section, we have shown that El Niño events cannot become huge in a warming  
359 climate in the GFDL-ESM2M, because the transient heating rate difference between the atmo-  
360 spheric and oceanic reservoirs enhances the cooling effect of the mean upwelling, which in turn  
361 damps the NDH necessary to produce a large positive eastern equatorial SST anomaly. In the

362 introduction section, we reviewed AJ04’s observational evidence that NDH causes the El Niño-  
363 La Niña amplitude asymmetry and that the NDH warming effect is comparable to LDH only for  
364 EENs. Therefore, due to the NDH dissipation, if El Niño events are weakened but La Niña events  
365 remains almost unchanged, then we expect a nonlinear rectification effect on the climatological  
366 mean state (Jin et al. 2003), which causes a La Niña-like mean-state SST response to global warm-  
367 ing.

368 Figures 6 (a) and (b) show the results of the idealized model runs with weak and strong green-  
369 house forcing. We use the parameters of  $Q_r = 1.0$  ( $^{\circ}\text{C}/\text{century}$ ) and  $Q_o = 0.3$  ( $^{\circ}\text{C}/\text{century}$ ) for  
370 the weak greenhouse forcing run (identical to Fig. 3b), and  $Q_r = 2.5$  ( $^{\circ}\text{C}/\text{century}$ ) and  $Q_o = 1.8$   
371 ( $^{\circ}\text{C}/\text{century}$ ) for the strong greenhouse forcing run. For both runs, we kept  $Q_r - Q_o$  (therefore  
372  $T_a - T_o$ ) the same,  $0.7$   $^{\circ}\text{C}/\text{century}$ , but only changed the magnitude of warming. As discussed in  
373 the last section, the key parameter for the importance of NDH is  $T_a - T_o$ , rather  $T_a$  or  $T_o$  individ-  
374 ually, so the nonlinear behaviors are reasonably similar between the two runs except for minor  
375 differences due to the chaotic nature of the dynamical system.

376 In both experiments, the warm pool SST (i.e, the MPI) warms with a strict upper bound of the  
377 radiative-convective equilibrium temperature. Comparing the first century (nonlinear regime) with  
378 the second century (linear regime), the mean-climate warm pool SST warms accordingly. On the  
379 other hand, because of the EEN dissipation at about Year100 (i.e.,  $T_a - T_o = 14.2$   $^{\circ}\text{C}$ ), the mean-  
380 state cold tongue SST experiences cooling (weak greenhouse forcing) or slow warming (strong  
381 greenhouse forcing) during the two centuries. In particular, it is interesting that global “warming”  
382 forcing by itself could even “cool” the eastern equatorial Pacific, if the forcing is not too strong.  
383 Of course, this cooling does not violate the second law of thermodynamics. The reason why the  
384 cold tongue SST cools is simply because the upwelling of the cool water stops being intermittently  
385 ceased in a warmer climate. Then, the strong greenhouse forcing run clearly shows that, even if

386 the EEN dissipation cooling effect is much weaker compared to the radiative warming, this effect  
387 is still detectable in the form of zonal difference of the warming rate.

388 In summary, the warm pool SST is almost solely bounded by the radiative convective equilib-  
389 rium temperature change, but the cold tongue SST is controlled by two competing effects between  
390 the radiative warming and the EEN-dissipation cooling. Therefore, at least in this idealized model,  
391 the western equatorial Pacific warms faster than the east due to a forced response to global warm-  
392 ing. We have hypothesized that this mechanism may be the cause of the La Niña-like mean-state  
393 warming in GFDL-ESM2M, or possibly, of part of the observed trend during the satellite era. We  
394 hereafter refer to this mechanism as Nonlinear ENSO Warming Suppression (NEWS), and will  
395 further explore whether it is actually realistic. The essential physics of the NEWS mechanism is  
396 that the increasing  $T_a - T_o$ , due to the transient heating rate difference between the atmospheric  
397 and oceanic reservoir, dissipates EENs due to the enhanced upwelling efficiency, and then as sug-  
398 gested by Jin et al. (2003), the weakened nonlinear ENSO amplitude causes a rectification cooling  
399 effect on the climatological-mean cold tongue SST.

400 The upper panel of Fig. 6 (c) shows the warm pool and cold tongue SST observed during  
401 DJF from 1965/66 through 2015/16. As we have already seen in Fig. 2, the nonlinear regime  
402 continued toward the end of the past century, and since then it has been almost linear. At least  
403 by this metric, the warm pool is warming much faster than the cold tongue (where the SST has  
404 slightly cooled), which is consistent with the NEWS mechanism. Though this mean cooling is  
405 undoubtedly exaggerated by natural variability, our point here is that, even if the cold tongue has  
406 been cooling during the past half a century, part of this trend in the tropical Pacific may be forced  
407 by global warming, as shown in Fig. 6 (a). Because of the zonal difference of the warming rate,  
408 the spatial pattern of the SST trend looks like a La Niña-like warming (Fig 6c, lower).

409 The GFDL-ESM2M is also consistent with NEWS. Figure 6 (d) shows the modeled warm pool  
410 and cold tongue SST during DJF in RCP 8.5. As we have seen in Fig. 4, the nonlinear regime  
411 appears to end in about 2070. This run looks more similar to the strong greenhouse forcing ex-  
412 periment in the idealized model (Fig. 6b). Because of the strong greenhouse forcing, one might  
413 have the impression that the NEWS effect appears to be subtle in the time series (Fig. 6d, upper).  
414 The spatial pattern of the trend (Fig. 6d, lower), however, undoubtedly shows that the west Pacific  
415 warms faster than the east, which is consistent with the NEWS mechanism.

416 *b. Necessary conditions of NEWS*

417 We expect that the atmospheric heating should be faster than the oceanic heating in most CMIP5  
418 models, not just the GFDL-ESM2M. Why, then, do the majority of the CMIP5 models lack the  
419 La Niña-like trend associated with NEWS? As shown in the idealized model experiments, the  
420 nonlinear dynamics of ENSO is an essential ingredient of NEWS. If GCMs do not capture realistic  
421 nonlinear ENSO dynamics, the NEWS mechanism cannot operate, which could have implications  
422 for the reliability (or lack thereof) of tropical mean-climate change projections by those models.

423 Figure 7 (a) shows a scatter plot of the relationship between the ENSO nonlinearity and the zonal  
424 SST gradient response to warming calculated for 32 CMIP5 models and observations. Here, the  
425 ENSO nonlinearity is defined as the skewness of detrended 11-month running mean SST anoma-  
426 lies, and is averaged over the Niño3 region so that positive skewness means larger El Niños and  
427 smaller La Niñas. The zonal SST gradient is defined as Niño3 SST anomalies minus Niño4 (5°S-  
428 5°N and 160°E-150°W) SST anomalies as in KHB16 so that a positive  $\Delta(\text{Niño3-Niño4})$  means an  
429 El Niño-like mean-state warming. Interestingly, the majority of the models exhibit little nonlin-  
430 earity of ENSO and El Niño-like warming trends, but observations and the GFDL-ESM2M both  
431 show large nonlinearity and La Niña-like warming trends. Therefore, it is possible that only the

432 GFDL-ESM2M can capture the Pacific SST response to warming in the real world. Comparing  
433 RCP 6.0 and 8.5, the larger zonal SST gradient change in the GFDL-ESM2M than in observations  
434 could partly be explained by the greenhouse warming strength, but it could also be attributed to  
435 the ENSO amplitude bias of GFDL-ESM2M (Figs. 7b and c).

436 Figures 7 (d) through (f) show some examples of detrended 11-month running mean Niño3 time  
437 series from the CMIP5 models. Figure 7 (d) shows three models, HadGEM2-CC, MPI-ESM-LR,  
438 and CSIRO-Mk3-6-0, which exhibit opposite or insufficient ENSO asymmetry compared to ob-  
439 servations. CSIRO-Mk3-6-0 has a strong warming near the Niño4 region, and therefore it exhibits  
440 an extremely negative  $\Delta(\text{Niño3-Niño4})$  (Fig. 7a). Nevertheless, the spatial pattern looks more  
441 like the multi-model mean El Niño-like pattern (not shown; qualitatively similar to the right panel  
442 of Fig. 8b). Figure 7 (e) shows two models, CESM1-CAM5, and IPSL-CM5A-MR, which ex-  
443 hibit better asymmetry. These models, however, do not have EENs that stand out among other El  
444 Niño events, which are also essential for the NEWS mechanism to work. An interesting outlier is  
445 MIROC 5 shown in Fig. 7 (f). This model is the only model that exhibits more realistic skewness  
446 than GFDL-ESM2M (Fig. 7a), but it also exhibits the largest positive  $\Delta(\text{Niño3-Niño4})$ , or a strong  
447 El Niño-like warming. The time series shows a large number of EENs, so it is possible that NDH  
448 in this model may be too large, more like the upper left panel of Fig. 3 (a) with small climatolog-  
449 ical  $T_a - T_o$ . Thus, it may be hard for  $T_a - T_o$  to surpass the threshold at which the importance of  
450 ENSO nonlinearity bifurcates. Further investigation is needed to understand why MIROC 5 does  
451 not simulate NEWS despite its realistic nonlinearity.

452 *c. Transient feature of NEWS and the direction of causality between the ENSO amplitude change*  
453 *and the mean-state trends*

454 Though we have used piControl and Abrupt4xCO<sub>2</sub> to show the EEN dissipation in the previous  
455 section, the rectification effect on the mean-state SST exhibits some important differences between  
456 a gradual CO<sub>2</sub> increase and an abrupt one. Figures 8 (a) and (b) show the spatial pattern of the SST  
457 trend relative to the Pacific mean trend for gradual and abrupt CO<sub>2</sub> increases. As we have discussed  
458 so far, the mean-state SST responses in the gradual CO<sub>2</sub> runs are clearly La Niña-like, which  
459 we believe are associated with NEWS. The warming response of the abrupt runs (expressed as  
460 Abrupt4xCO<sub>2</sub> minus piControl), however, exhibits more zonally uniform warming. If we look at  
461 this pattern carefully, the west Pacific exhibits a reasonably similar spatial structure to the gradual  
462 runs, but it also exhibits additional warming anomalies in the east.

463 The 300-year trends calculated for Abrupt4xCO<sub>2</sub> might uncover the cause (Fig. 8b, right). The  
464 spatial structure of this trend pattern looks quite similar to the multi-model mean calculated for  
465 CMIP5 (Ying et al. 2016; Zheng et al. 2016). Given that this multi-model-mean El Niño-like  
466 pattern is associated with the slow response of the Walker Circulation change (Held and Soden  
467 2006; Vecchi and Soden 2007; Held et al. 2010) or the ocean dynamics (Luo et al. 2015), the  
468 spatial pattern of the “Abrupt4xCO<sub>2</sub> minus piControl” could be interpreted as the superposition  
469 of the slow El Niño-like pattern and the transient La Niña-like pattern associated with NEWS.  
470 This idea of superposition is consistent with the fact that the trends shown in the second century of  
471 1pctCO<sub>2</sub> run is overall weaker than those shown in the first century, because the NEWS mechanism  
472 is slow but transient, and that the trend pattern calculated for the full two centuries in 1pctCO<sub>2</sub> does  
473 not look too different from the “Abrupt4xCO<sub>2</sub> minus piControl” (not shown).

474 We have to remember, however, that the CO<sub>2</sub> increase in the real world should be gradual,  
475 not abrupt. Therefore, at least based on these results from the GFDL-ESM2M, the realistic SST  
476 warming pattern during this century should be closer to the La Niña-like one associated with the  
477 transient NEWS mechanism. Some previous studies (e.g., Held et al. 2010) have shown that the La  
478 Nina-like fast response to abrupt CO<sub>2</sub> forcing might be due to the Ocean Dynamical Thermostat  
479 (Clement et al. 1996). The response time scale of the Ocean Dynamical Thermostat, however,  
480 is too short to appear in the centennial trend of the gradual warming runs, because the shallow  
481 oceanic overturning circulation that largely controls the thermostat mechanism takes only about a  
482 couple of decades at the longest to complete its full circuit and to reach quasi-equilibrium.

483 The different response between the gradual and abrupt runs might also help elucidate the direc-  
484 tion of causality between the EEN dissipation and the mean-state SST change. As we have shown,  
485 in the Abrupt4xCO<sub>2</sub> run, the mean-state warming response is zonally uniform because the slow  
486 El Niño-like response also contributes to the total trend. Interestingly, however, the ENSO am-  
487 plitude still keeps its weakened amplitude, without any EENs, even in late third century (Fig. 4).  
488 This weakened amplitude means that the ENSO amplitude is not affected by the zonally-uniform  
489 mean-state change in the abrupt run. Therefore, at least in the GFDL-ESM2M, the ENSO ampli-  
490 tude suppression is more likely to be a cause, rather than an effect, of the La Niña-like mean-state  
491 change in the gradual CO<sub>2</sub> increase runs. This result questions the views presented in some ear-  
492 lier studies that treated ENSO as more like a linear mode (e.g., Timmermann et al. 1999; An and  
493 Jin 2000; Fedorov and Philander 2000; Urban et al. 2000; Wang and An 2001, 2002), but is con-  
494 sistent with a submitted work by Atwood et al. (2016) where they took nonlinearity into account  
495 (available at [http://www.atmos.washington.edu/~david/Atwood\\_etal\\_ENSO\\_submitted\\_](http://www.atmos.washington.edu/~david/Atwood_etal_ENSO_submitted_2016.pdf)  
496 2016.pdf). Closer investigation is needed to further verify the causality.

497 *d. The Pacific mean-state climate change as a forced response to global warming*

498 Figure 9 presents three warming scenarios that can be simulated by state-of-the-art GCMs. Fig-  
499 ure 9 (a) shows the NEWS scenario, where gradual global warming increases  $T_a - T_o$  and trig-  
500 gers the transient NEWS mechanism to yield a La Niña-like trend (Fig. 8a). To the best of our  
501 knowledge, this scenario is only simulated by the GFDL-ESM2M, which exhibits the second most  
502 realistic ENSO nonlinearity among the 32 CMIP5 models investigated here. As shown by KHB16  
503 in their Fig. 3, the La Niña-like trend then strengthens the Walker circulation, whose structure  
504 is remarkably similar to the observed trend during the satellite era. Because the NEWS effect  
505 is so strong, the GFDL-ESM2M does not use the Walker circulation for weakening the global-  
506 mean atmospheric circulations to sustain the energy and water balance (Held and Soden 2006),  
507 as the majority of GCMs do (Vecchi and Soden 2007). Nevertheless, KHB16 also showed that  
508 the energy-water balance in the GFDL-ESM2M is still sustained in the global mean, which is still  
509 consistent with Held and Soden (2006). Therefore, unlike the majority of the CMIP5 models, it is  
510 virtually certain that the GFDL-ESM2M, rather than weakening the Walker circulation, weakens  
511 the atmospheric circulation in some other region(s), which could be interesting to investigate fur-  
512 ther. On the other hand, the reason why the majority of the CMIP5 models do not simulate NEWS  
513 appears to be that the ENSO nonlinearity of these models is unrealistic (Figs. 7 and 9b).

514 Figure 9 (c) shows the Abrupt Warming scenario, where  $\text{CO}_2$  is abruptly increased instanta-  
515 neously. Even for the abrupt increase, the increase of  $T_a - T_o$  dissipates EENs as shown in Fig. 1,  
516 so the NEWS mechanism must work. The mean-state SST rectification effect of NEWS, however,  
517 appears to be masked by other mechanisms as follows. First, because of the short time span of the  
518  $\text{CO}_2$  increase, the effect of Ocean Dynamical Thermostat (Clement et al. 1996) might dominate  
519 the fast SST response as suggested by Held et al. (2010). Moreover, once the system reaches its

520 quasi-equilibrium, the energy-water balance eventually starts to weaken the Walker Circulation  
521 as a slow response, which helps an El Niño-like trend emerge (Fig. 8b, right). It is also pos-  
522 sible that the ocean dynamics could also contribute to the El Niño-like trend, as recently shown  
523 by Luo et al. (2015). Therefore, by subtracting the piControl climatology from the equilibrated  
524 Abrupt4xCO<sub>2</sub> climatology, we detect a superposition of the La Niña-like trend caused by the tran-  
525 sient mechanisms and the El Niño-like trend caused by the energy-water balance, which is a more  
526 zonally-uniform SST warming (Fig. 8b). Despite the zonally-uniform mean-state SST change, the  
527 ENSO amplitude is kept suppressed in a warmer climate (Fig. 1). Therefore, it is more likely that  
528 that the weakening ENSO amplitude under gradual warming is a cause, rather than an effect, of  
529 the mean-state SST change.

## 530 **5. Implications for multi-decadal natural variability of the Pacific SST and global warming**

### 531 **hiatuses**

532 Because the NEWS mechanism is driven by the reservoir temperature difference between the  
533 atmosphere and ocean, the root cause of this difference does not have to be greenhouse forcing,  
534 as long as the Earth is transiently heated and the lower atmosphere warms faster than the oceanic  
535 interior. Therefore, even if the Earth is warmed by natural variability, rather than an anthropogenic  
536 forcing, the NEWS mechanism should still operate. The opposite mechanism might also work if  
537 the Earth is cooled by a certain cause. In this section, we further explore the idealized model and  
538 the piControl run to investigate some implications of NEWS for multi-decadal natural variability  
539 of the Pacific SST. We then discuss the effect of this natural variability on global warming.

540 *a. IPO-like natural multi-decadal variability explained by the NEWS-NEWA cycle*

541 If the Earth's atmosphere were cooled by a random natural cause, this cooling would transiently  
542 decrease  $T_a - T_o$ , making upwelling less efficient and producing more EENs with nonlinear ENSO  
543 dynamics. The increased number of EENs must then have a rectification warming effect on the  
544 mean-state cold tongue SST, producing an El Niño-like mean climate. If the NEWS mechanism  
545 is realistic, this opposite mechanism should also operate. Hereafter, we refer to this mechanism as  
546 the Nonlinear ENSO Warming Acceleration (NEWA).

547 Moreover, as Kosaka and Xie (2013) and many others have discussed in relation to the recent  
548 global warming slowdown, it is known that a prolonged La Niña-like mean-state cools the atmo-  
549 spheric temperature, and vice versa. Therefore, we expect that the effect of NEWS (NEWA) can  
550 eventually cause NEWA (NEWS), and the repetition of NEWS and NEWA might contribute to  
551 multi-decadal natural variability. The idea can be summarized into five steps as follows:

- 552 1. When the atmosphere is warmed, the NEWS mechanism yields a La Niña-like Pacific mean  
553 climate.
- 554 2. The prolonged La Niña-like Pacific mean climate eventually cools the atmosphere.
- 555 3. When the atmosphere is cooled, the NEWA mechanism yields an El Niño-like Pacific mean  
556 climate.
- 557 4. The prolonged El Niño-like Pacific mean climate eventually warms the atmosphere.
- 558 5. Repeat 1-4.

559 Based on this idea, we have further generalized the idealized model by making the atmospheric  
560 reservoir temperature sensitive to the cold tongue SST as described in section 2. In this model,  
561 the atmosphere has also its normal mode of natural variability that restores the atmosphere toward

562 the radiative-convective equilibrium temperature, and is forced by the cold tongue SST. Figure  
563 10 (a) shows the warm pool and cold tongue SST simulated by the idealized model. Because  
564 of the forced oscillation of the atmospheric reservoir temperature,  $T_a - T_o$  exhibits a sinusoidal  
565 variation so that it crosses the threshold that bifurcates the importance of the ENSO nonlinearity  
566 (i.e.,  $T_a - T_o = 14.2$  °C). Therefore, during a nonlinear ENSO phase, EENs emerge and suppress  
567 the cooling rate of the atmosphere by the cold tongue. The resulting warming pushes the system  
568 toward a linear ENSO phase by the NEWS mechanism. On the other hand, during a linear ENSO  
569 phase, EENs dissipate, and the cold tongue enhances the cooling rate of the atmosphere. The  
570 resulting cooling pushes the system toward a nonlinear ENSO phase by the NEWA mechanism.  
571 This NEWS-NEWA cycle exhibits a clear multi-decadal oscillation that is reasonably similar to  
572 the Interdecadal Pacific Oscillation (IPO) observed in the real world.

573 Next, it would be interesting to investigate if the GFDL-ESM2M reproduces this NEWS-NEWA  
574 cycle. By taking a careful look at the piControl run shown in Fig. 4, one finds that NDH and EENs  
575 are weakened during about Year  $300 \pm 50$ . Therefore, we hypothesize that this amplitude variation  
576 might be understood in the context of the NEWS-NEWA cycle. Figures 10 (b) and (c) show the  
577 warm pool and cold tongue SST,  $T_a - T_o$ , and the SST trend pattern during Year 211-400. During  
578 the first half of this period (Fig. 10b),  $T_a - T_o$  has a clear positive trend, EENs dissipate in about  
579 Year 260, and the Pacific SST exhibits a La Niña-like trend. Therefore, the first half of the period  
580 is consistent with the NEWS mechanism as described in the previous section. On the other hand,  
581 during Year 306-400 (Fig. 10c), a negative trend of  $T_a - T_o$ , an increasing number of EENs, and  
582 an El Niño-like trend are detected, which is consistent with the NEWA mechanism.

583 Because the normal mode frequency of the atmospheric natural variability ( $\omega$ ) and the sensi-  
584 tivity of atmospheric heating rate to the cold tongue SST ( $\gamma$ ) are free parameters that are difficult  
585 to estimate based on currently available observational records, the above-mentioned mechanism

586 remains speculative. A more rigorous heat budget analysis is also needed to confirm that the natu-  
587 ral  $T_a - T_o$  variation in the GFDL-ESM2M is induced by the modulation of heating by the Pacific  
588 mean-state SST variations. Nevertheless, the mechanism makes physical sense, so it is expected  
589 to contribute to the observed IPO-like multi-decadal SST variability at least to some extent. The  
590 remarkable resemblance between the idealized model and the GFDL-ESM2M also increases the  
591 interest in investigating this NEWS-NEWA hypothesis further as one of many possible mecha-  
592 nisms of low frequency natural SST variability, such as the IPO. It is also consistent with previous  
593 studies that suggested that EENs may play a role in changing the phase of the IPO (e.g., Meehl  
594 et al. 2016). Model-based process studies using GCMs, and if possible, observational verifications  
595 might shed new light on our understanding of the tropical Pacific multi-decadal natural variability.

#### 596 *b. Implications for global warming hiatuses*

597 The main idea of Kosaka and Xie (2013) was to explain the recent global warming slowdown  
598 by prescribing the Pacific multi-decadal SST variability. Therefore, if we hypothesize that the  
599 NEWS-NEWA cycle explains a certain variance of the Pacific low-frequency natural SST vari-  
600 ability, one straightforward societal application of the NEWS-NEWA cycle may be an attempt  
601 to explain global warming hiatuses. In this subsection, we further investigate global warming  
602 hiatuses using the idealized model and compare them to the observed global warming hiatuses.

603 Figure 11 (a) shows the atmospheric natural variability simulated by the idealized model with  
604 zero sensitivity to the cold tongue SST. The heating rate of radiative-convective equilibrium tem-  
605 perature and oceanic reservoir temperature are chosen to be  $Q_r = 2.0$  °C/century and  $Q_o = 1.9$   
606 °C/century, respectively. The atmospheric reservoir temperature is strongly restored toward the  
607 prescribed, increasing radiative-convective equilibrium temperature that serves as an analog of  
608 greenhouse forcing. From this simulation, it is confirmed that, though the atmospheric tempera-

609 ture exhibits weak oscillations and slowdowns, occasional negative decadal trends such as those  
610 observed in the real world are not simulated solely by the atmospheric natural variability under the  
611 parameter values and initial conditions used here.

612 Next, as described in section 2, we have allowed ocean-atmosphere interaction to operate in the  
613 idealized model. Figure 11 (b) shows the result of this simulation. Because the atmosphere is sen-  
614 sitive to the cold tongue SST, the model exhibits well-defined hiatus periods where the atmospheric  
615 temperature does not experience a monotonic increase. It is consistent with the NEWS-NEWA cy-  
616 cle that the warming trend of the atmospheric temperature is boosted by the emergence of EENs  
617 at the end of the hiatus periods, and is moderated by the absence of EENs during the prolonged  
618 linear ENSO phase. As a feature of the forced oscillation, the frequency of the atmospheric vari-  
619 ability is slightly modulated by the IPO-like multi-decadal SST variability. For the ocean, on the  
620 other hand, relatively large variations of  $T_a - T_o$  forced originally by the low-frequency variations  
621 of EENs, are in turn necessary to repeatedly cross the threshold temperature (i.e.,  $T_a - T_o = 14.2$   
622 °C) to maintain the low-frequency variations of the NDH and EENs. If this is the case, both atmo-  
623 spheric and oceanic roles are important for simulating the emergence and termination of multiple  
624 hiatus periods, instead of the atmosphere being unidirectionally forced by the “prescribed” SST  
625 multi-decadal variability. In addition, considering that the key metric of the NEWS-NEWA cycle  
626 is the ENSO nonlinearity, the lack of realistic ENSO nonlinearity may be one of many reasons why  
627 most GCMs do not reproduce the recent global warming slowdown, at least without prescribing  
628 observed SSTs (Kosaka and Xie 2013) or trade winds (Watanabe et al. 2014) in the eastern Pacific.

629 Though the data quality of the observational datasets is limited before the middle of the past  
630 century, we have further attempted to compare this result to observations. Figure 11 (c) shows the  
631 annual-mean, global-mean surface temperature time series in place of the atmospheric reservoir,  
632 and SST (the warm pool and cold tongue SST) during DJF of 1880-2015. Overall, the qualitative

633 features are similar to the results simulated by the idealized model. Particularly similar is the  
634 feature that the EENs in 1982/83 and 1997/98 (and possibly 1972/73) appear to have boosted the  
635 global warming trend during the early satellite era, which is also consistent with previous studies  
636 suggesting a relationship between global warming hiatuses and IPO phase changes. Based on the  
637 idea of the NEWS-NEWA cycle, we also expect some EENs during about 1910-1930, which were  
638 not as clearly observed as during the early satellite era. It is also possible, however, that the lack  
639 of EENs during 1910-1930 is, in part, due to the relatively poor data quality during this period.

## 640 **6. Conclusions**

641 In this study, we have investigated observational data and model output from an idealized non-  
642 linear recharge oscillator model and GCMs (with an emphasis on the GFDL-ESM2M) to obtain  
643 the following conclusions.

644 *a. A nonlinear theory shows that extreme El Niño (EEN) events may currently be becoming less  
645 frequent, and if global warming continues, EENs may not be observed at the end of this century.*

646 *At least one GCM is consistent with this theory.*

647 Some earlier studies that suggested an increase of the ENSO variance under global warming  
648 treated ENSO as a linear mode. This study, on the other hand, incorporates nonlinear ENSO dy-  
649 namics and reconsiders future changes to ENSO. In our idealized model and the GFDL-ESM2M  
650 (which has the second-most realistic ENSO nonlinearity of the 32 CMIP5 models investigated  
651 here), the ENSO amplitude weakens substantially in a warmer climate. Due to the transient heat-  
652 ing rate difference between the atmospheric and oceanic reservoir, the upwelling efficiency tends  
653 to become enhanced under global warming. When the reservoir temperature difference (and there-  
654 fore upwelling cooling efficiency) surpasses a certain threshold, the equatorial thermocline cannot

655 recharge the heat enough to collapse the climatological mean state, such that the nonlinear heating  
656 effect works to yield EENs (Figs. 1 through 5).

657 When the system approaches the threshold, the idealized model and the GFDL-ESM2M predict  
658 that EENs become less frequent (Figs. 3 and 4). Though we do not have enough observational  
659 evidence to verify this behavior, it is at least consistent with the available observational evidence  
660 that relatively large El Niño events were observed in 1972/73, 1982/83, 1997/98, and 2015/16, and  
661 thus the interval between events has increased from 10, to 15, to 18 years. Based on this idea, one  
662 might speculate that the next large El Niño event may perhaps occur around 2035/36, although  
663 other chaotic variability and forcings may work to the contrary. If global warming continues, the  
664 theory further predicts that ENSO becomes more linear and that EENs might not be observed at  
665 the end of this century.

666 *b. A reasonable La Niña-like warming scenario can be outlined by the Nonlinear ENSO Warming*  
667 *Suppression (NEWS) mechanism as a forced response to global warming.*

668 The forced weakening of ENSO amplitude has a rectifying cooling effect on the mean-state  
669 cold tongue SST (Fig. 6). Due to the nonlinear heating effect, the number of large El Niño  
670 events decreases while the number of La Niña events remains nearly constant. Therefore, the  
671 mean climate becomes La Niña-like. This nonlinear rectification effect by itself is essentially  
672 opposite to the effect that Jin et al. (2003) showed for the strengthening ENSO amplitude and the  
673 warming cold tongue SST. The novelty of the NEWS mechanism is that the weakening ENSO  
674 can be explained as a forced response to global warming (Conclusion *a*), which then yields the La  
675 Niña-like mean state by the nonlinear rectification effect.

676 *c. NEWS is different from the Ocean Dynamical Thermostat*

677 Some earlier studies at the end of the past century showed that the forced response should be  
678 La Niña-like, because the climatological upwelling cooling effect will compensate the radiative  
679 warming in the east but not in the west (Cane et al. 1997). This mechanism is called the Ocean  
680 Dynamical Thermostat (Clement et al. 1996). The mechanism is, however, now thought to be  
681 incapable of explaining a centennial trend, because the upwelling water in the cold tongue becomes  
682 warmer and reaches equilibrium after only a couple of decades, when the warmed extratropical  
683 surface water arrives in the equatorial thermocline through the upper oceanic subtropical cell.

684 The NEWS mechanism is essentially different from the Ocean Dynamical Thermostat. One  
685 important difference is the time scale of the La Niña-like warming. Because the NEWS mechanism  
686 takes time for multiple EENs to dissipate, it requires almost a full century to produce the mature  
687 La Niña-like trend (see also Fig. 2 in KHB16). This is different from the Ocean Dynamical  
688 Thermostat, which takes less than a couple of decades at the slowest. The NEWS mechanism also  
689 involves nonlinear ENSO dynamics, whereas the Ocean Dynamical Thermostat does not invoke  
690 ENSO at all.

691 *d. The well-known El Niño-like mean-state warming is only a “majority decision” based on cur-*  
692 *rently available GCMs, most of which exhibit unrealistic nonlinearity of the ENSO dynamics.*

693 *A particularly important metric that needs urgent improvement in GCMs is the ENSO nonlin-*  
694 *earity.*

695 The majority of the CMIP5 models exhibit an El Niño-like mean-state warming. Therefore,  
696 widely believed by the ENSO research community is that the warming response is more likely to be  
697 El Niño-like. We have shown here, however, this could be just a “majority decision” by the GCMs

698 with unrealistic ENSO nonlinearity (Fig. 7). To the best of our knowledge, only one state-of-  
699 the-art GCM, the GFDL-ESM2M, simulates the La Niña-like warming by the NEWS mechanism.  
700 Nevertheless, based on the realistic ENSO nonlinearity of this model and the remarkable structural  
701 resemblance of the Walker circulation change to that of observations (Fig. 3 in KHB16), we  
702 believe this may be an equally realistic (or even more plausible) response to warming. Further  
703 investigation is needed using some of the new GCMs in upcoming CMIP phases, which we hope  
704 will better reproduce the observed ENSO nonlinearity. KHB16 pointed out that the La Niña-  
705 like warming might be related to the upper ocean diffusivity and thermal stratification; improving  
706 these upper ocean properties might solve the problems of the unrealistic nonlinearity evident in  
707 most CMIP5 models.

708 *e. Even for a first-order problem, “Warmer minus Control” is not necessarily a good analogue of*  
709 *a gradual global warming.*

710 Our results show that the La Niña-like warming happens only when the greenhouse forcing is  
711 increased gradually (Fig. 8). In the abrupt increase of CO<sub>2</sub>, the warming response is more like  
712 a zonally uniform warming, due to the influence of a slow El Niño-like response in addition to  
713 the transient NEWS mechanism (Fig. 9). Therefore, we should emphasize that “Warmer minus  
714 Control”, which is often used in global warming research, is not necessarily a good analogue of a  
715 gradual global warming even for a first-order feature of GCMs, if the response could be transient.

716 *f. At least in the GFDL-ESM2M, the ENSO amplitude variation appears to be a cause, rather than*  
717 *an effect, of the mean-state SST variation.*

718 Interestingly, even if the mean climate experiences a zonally uniform warming (Conclusion *e*),  
719 the ENSO amplitude has no dependence on the mean-state SST change in a warmer climate (Figs.

720 1 and 4). Therefore, it is more reasonable to assume that the ENSO amplitude variation in the  
721 GFDL-ESM2M is a cause, rather than an effect, of the mean-state SST variation. This direction  
722 of causality is important for the NEWS mechanism to dominate the global warming response, so  
723 further rigorous verifications are needed.

724 *g. EENs might better be treated as a completely different phenomenon than the linear ENSO mode.*

725 Some earlier studies regarded ENSO as a linear mode and predicted an increase of ENSO vari-  
726 ance under global warming. If nonlinear ENSO dynamics are taken into account, however, one  
727 reaches the conclusion that ENSO variance should *decrease*. Because EENs have huge amplitudes  
728 compared to the linear ENSO mode, we expect the teleconnections to the extratropical regions  
729 should also be substantially different. For example, the area with SST warmer than 28°C (the  
730 threshold at which deep convection can occur in the current climate) is much larger in EENs. This  
731 large area cannot be described as a linear perturbation from the climatological mean, as suggested  
732 in Fig. 2. Many other features that have been believed to be typical for ENSO could be made  
733 radically different by the nonlinearity of EENs. Further investigation is needed to shed light on  
734 the abnormality of EENs compared to the known linear ENSO mode.

735 *h. Understanding EENs may aid the understanding of Pacific multi-decadal natural variability*  
736 *and change. NEWS-NEWA cycle serves as one of many possibilities.*

737 We have also introduced the opposite mechanism to NEWS, the Nonlinear ENSO Warming  
738 Acceleration (NEWA), by which “global cooling” suppresses the upwelling efficiency, excites  
739 EENs, and yields an El Niño-like warming. Because a La Niña-like (El Niño-like) mean state  
740 eventually cools (warms) the Earth, the effect of NEWS can excite NEWA, and vice versa. Though  
741 whether this NEWS-NEWA cycle operates in the real world remains speculative, our idealized

742 model and the GFDL-ESM2M suggest that this NEWS-NEWA cycle may partly contribute to the  
743 multi-decadal natural SST variability in the Pacific (Fig. 10), including the Interdecadal Pacific  
744 Oscillation (IPO), whose phase change is thought to be causally related to an occurrence of a large  
745 El Niño (e.g., Meehl et al. 2016).

746 Some previous studies suggest that global warming hiatuses or slowdowns may be related to the  
747 multi-decadal variability of Pacific SSTs (e.g., Kosaka and Xie 2013). If the IPO can be partially  
748 explained by the NEWS-NEWA cycle, then both atmospheric and oceanic roles must be important  
749 to understand the hiatuses in relation to nonlinear ENSO dynamics (Fig. 11). If the nonlinearity  
750 plays a role in producing the Pacific multi-decadal variability, global warming hiatuses should not  
751 be understood as a unidirectionally forced response of the atmosphere to the “prescribed” SST  
752 variations, but rather, as two-way ocean-atmosphere interaction between the global mean atmo-  
753 spheric reservoir and the Pacific cold tongue. To realistically simulate global warming hiatuses,  
754 state-of-the-art GCMs may require further improvements to their ENSO nonlinearity.

755 *Acknowledgments.* The work was supported by the National Science Foundation (NSF) un-  
756 der Grant AGS-0960497 and the first author’s work is also supported by NSF under Grant  
757 AGS-1122989, Takenaka Scholarship Foundation, and Iizuka Takeshi Scholarship Foundation.  
758 We would like to thank Casey Hilgenbrink for correcting English grammar of the first draft.  
759 Isaac Held’s Blog post #45 ([http://www.gfdl.noaa.gov/blog/isaac-held/2014/04/24/  
760 45-dynamic-retardation-of-tropical-warming/](http://www.gfdl.noaa.gov/blog/isaac-held/2014/04/24/45-dynamic-retardation-of-tropical-warming/)) was a useful reference for this study.

## 761 **References**

762 An, S.-I., and F.-F. Jin, 2000: An eigen analysis of the interdecadal changes in the structure and  
763 frequency of ENSO mode. *Geophys. Res. Lett.*, **27** (16), 2573–2576.

- 764 An, S.-I., and F.-F. Jin, 2004: Nonlinearity and asymmetry of ENSO. *J. Climate*, **17** (12), 2399–  
765 2412.
- 766 An, S.-I., J.-W. Kim, S.-H. Im, B.-M. Kim, and J.-H. Park, 2012: Recent and future sea surface  
767 temperature trends in tropical Pacific warm pool and cold tongue regions. *Climate Dyn.*, **39** (6),  
768 1373–1383.
- 769 Behringer, D., and Y. Xue, 2004: Evaluation of the global ocean data assimilation system at NCEP:  
770 The Pacific Ocean. *Proc. Eighth Symp. on Integrated Observing and Assimilation Systems for*  
771 *Atmosphere, Oceans, and Land Surface*.
- 772 Cane, M. A., A. C. Clement, A. Kaplan, Y. Kushnir, D. Pozdnyakov, R. Seager, S. E. Zebiak, and  
773 R. Murtugudde, 1997: Twentieth-century sea surface temperature trends. *Science*, **275** (5302),  
774 957–960.
- 775 Christensen, J., and Coauthors, 2013: *Climate Phenomena and their Relevance for Future Re-*  
776 *gional Climate Change*, book section 14, 1217–1308. Cambridge University Press, Cambridge,  
777 United Kingdom and New York, NY, USA, doi:10.1017/CBO9781107415324.028.
- 778 Clement, A. C., R. Seager, M. A. Cane, and S. E. Zebiak, 1996: An ocean dynamical thermostat.  
779 *J. Climate*, **9** (9), 2190–2196.
- 780 Collins, M., and Coauthors, 2005: El Niño-or La Niña-like climate change? *Climate Dyn.*, **24** (1),  
781 89–104.
- 782 Collins, M., and Coauthors, 2010: The impact of global warming on the tropical Pacific Ocean  
783 and El Niño. *Nature Geosci.*, **3** (6), 391–397.
- 784 Fedorov, A. V., and S. G. Philander, 2000: Is El Niño changing? *Science*, **288** (5473), 1997–2002.

- 785 Hansen, J., R. Ruedy, M. Sato, and K. Lo, 2010: Global surface temperature change. *Rev. Geo-*  
786 *phys.*, **48** (4).
- 787 Held, I. M., and B. J. Soden, 2006: Robust responses of the hydrological cycle to global warming.  
788 *J. Climate*, **19** (21), 5686–5699.
- 789 Held, I. M., M. Winton, K. Takahashi, T. Delworth, F. Zeng, and G. K. Vallis, 2010: Probing the  
790 fast and slow components of global warming by returning abruptly to preindustrial forcing. *J.*  
791 *Climate*, **23** (9), 2418–2427.
- 792 Jin, F.-F., 1996: Tropical ocean-atmosphere interaction, the Pacific cold tongue, and the El Niño-  
793 Southern Oscillation. *Science*, **274** (5284), 76.
- 794 Jin, F.-F., 1997: An equatorial ocean recharge paradigm for ENSO. Part I: Conceptual model. *J.*  
795 *Atmos. Sci.*, **54** (7), 811–829.
- 796 Jin, F.-F., 1998: A simple model for the Pacific cold tongue and ENSO. *J. Atmos. Sci.*, **55** (14),  
797 2458–2469.
- 798 Jin, F.-F., S.-I. An, A. Timmermann, and J. Zhao, 2003: Strong El Niño events and nonlinear  
799 dynamical heating. *Geophys. Res. Lett.*, **30** (3).
- 800 Knutson, T. R., and S. Manabe, 1995: Time-mean response over the tropical Pacific to increased  
801 CO<sub>2</sub> in a coupled ocean-atmosphere model. *J. Climate*, **8** (9), 2181–2199.
- 802 Kohyama, T., and D. L. Hartmann, 2016: Antarctic sea ice response to weather and climate modes  
803 of variability. *J. Climate*, **29** (2), 721–741.
- 804 Kosaka, Y., and S.-P. Xie, 2013: Recent global-warming hiatus tied to equatorial Pacific surface  
805 cooling. *Nature*, **501** (7467), 403–407.

- 806 Luo, Y., J. Lu, F. Liu, and W. Liu, 2015: Understanding the El Niño-like oceanic response in the  
807 tropical Pacific to global warming. *Climate Dyn.*, **45 (7-8)**, 1945–1964.
- 808 Meehl, G. A., A. Hu, and H. Teng, 2016: Initialized decadal prediction for transition to positive  
809 phase of the Interdecadal Pacific Oscillation. *Nat. Commun.*, **7**.
- 810 Rayner, N., D. E. Parker, E. Horton, C. Folland, L. Alexander, D. Rowell, E. Kent, and  
811 A. Kaplan, 2003: Global analyses of sea surface temperature, sea ice, and night marine  
812 air temperature since the late nineteenth century. *J. Geophys. Res.*, **108 (D14)**, 4407, doi:  
813 10.1029/2002JD002670.
- 814 Smith, T. M., R. W. Reynolds, T. C. Peterson, and J. Lawrimore, 2008: Improvements to NOAA’s  
815 historical merged land-ocean surface temperature analysis (1880-2006). *J. Climate*, **21 (10)**,  
816 2283–2296.
- 817 Taylor, K. E., R. J. Stouffer, and G. A. Meehl, 2012: An overview of CMIP5 and the experiment  
818 design. *Bull. Amer. Meteor. Soc.*, **93 (4)**, 485–498.
- 819 Timmermann, A., F.-F. Jin, and J. Abshagen, 2003: A nonlinear theory for El Niño bursting. *J.*  
820 *Atmos. Sci.*, **60 (1)**, 152–165.
- 821 Timmermann, A., J. Oberhuber, A. Bacher, M. Esch, M. Latif, and E. Roeckner, 1999: Increased  
822 El Niño frequency in a climate model forced by future greenhouse warming. *Nature*, **398 (6729)**,  
823 694–697.
- 824 Urban, F. E., J. E. Cole, and J. T. Overpeck, 2000: Influence of mean climate change on climate  
825 variability from a 155-year tropical Pacific coral record. *Nature*, **407 (6807)**, 989–993.
- 826 Vecchi, G. A., and B. J. Soden, 2007: Global warming and the weakening of the tropical circula-  
827 tion. *J. Climate*, **20 (17)**, 4316–4340.

- 828 Waliser, D. E., and N. E. Graham, 1993: Convective cloud systems and warm-pool sea surface tem-  
829 peratures: Coupled interactions and self-regulation. *J. Geophys. Res.*, **98 (D7)**, 12 881–12 893.
- 830 Wang, B., and S. An, 2002: A mechanism for decadal changes of ENSO behavior: Roles of  
831 background wind changes. *Climate Dyn.*, **18 (6)**, 475–486.
- 832 Wang, B., and S.-I. An, 2001: Why the properties of El Niño changed during the late 1970s.  
833 *Geophys. Res. Lett.*, **28 (19)**, 3709–3712.
- 834 Watanabe, M., H. Shiogama, H. Tatebe, M. Hayashi, M. Ishii, and M. Kimoto, 2014: Contribution  
835 of natural decadal variability to global warming acceleration and hiatus. *Nat. Clim. Change*,  
836 **4 (10)**, 893–897.
- 837 Xie, S.-P., C. Deser, G. A. Vecchi, J. Ma, H. Teng, and A. T. Wittenberg, 2010: Global warming  
838 pattern formation: sea surface temperature and rainfall. *J. Climate*, **23 (4)**, 966–986.
- 839 Ying, J., P. Huang, and R. Huang, 2016: Evaluating the formation mechanisms of the equatorial  
840 Pacific SST warming pattern in CMIP5 models. *Adv. Atmos. Sci.*, **33 (4)**, 433–441.
- 841 Yokoi, S., and Y. N. Takayabu, 2009: Multi-model projection of global warming impact on tropical  
842 cyclone genesis frequency over the western north pacific. *J. Meteor. Soc. Japan*, **87 (3)**, 525–  
843 538, doi:10.2151/jmsj.87.525.
- 844 Zebiak, S. E., and M. A. Cane, 1987: A model El Niño-Southern Oscillation. *Mon. Wea. Rev.*,  
845 **115 (10)**, 2262–2278.
- 846 Zheng, X.-T., S.-P. Xie, L.-H. Lv, and Z.-Q. Zhou, 2016: Inter-model uncertainty in ENSO ampli-  
847 tude change tied to Pacific ocean warming pattern. *J. Climate*, *in press*.

848 **LIST OF FIGURES**

- 849 **Fig. 1.** Top panel, Sea surface temperature (SST) averaged over December-January-February (DJF),  
850 simulated by GFDL-ESM2M under the preindustrial control (piControl) and abrupt quadrupling  
851 carbon dioxide (Abrupt4xCO<sub>2</sub>) scenarios. Red curves show the SST time series averaged  
852 over the western warm pool (5°S-5°N, 130°E-160°E), and the blue curves show those  
853 of the eastern cold tongue (5°S-5°N, 120°W-90°W). For Abrupt4xCO<sub>2</sub>, only after Year100  
854 is shown because it takes several decades before the system reaches its quasi-equilibrium.  
855 Middle and Bottom panels, Nonlinear Dynamical Heating (NDH; middle) and Linear Dy-  
856 namical Heating (LDH; bottom) time series calculated using equation (1) for the same model  
857 runs as in the top panel, averaged over 5°S-5°N, 170°W-100°W. 3-month running mean is  
858 applied to both time series. . . . . 42
- 859 **Fig. 2.** (a): Left panel, Observed SST climatology during December-January-February (DJF). Con-  
860 tour interval is 1°C. Right panel, As in left, but for 1997/98 DJF. (b): As in (a), but for  
861 observed upper ocean potential temperature. (c): As in Fig. 1, but for observations. . . . . 43
- 862 **Fig. 3.** (a): As in the top and middle panels in Fig. 1, but for the idealized model. Each panel  
863 shows a simulation with fixed temperature difference between the atmospheric and oceanic  
864 reservoir ( $T_a - T_o$ ) indicated at the top left. (b): As in (a), but increasing  $T_a - T_o$  following  
865 the equation shown at the top left. The dashed line shows the time when  $T_a - T_o$  reaches the  
866 threshold that bifurcates the importance of the ENSO nonlinearity. . . . . 44
- 867 **Fig. 4.** As in the top and middle panels of Fig. 1, but panels for RCP 8.5 scenario is inserted between  
868 piControl and Abrupt4xCO<sub>2</sub>. The scale of the horizontal axes for RCP 8.5 is expanded by a  
869 factor of 2. Also shown at the bottom is 15-year running mean  $T_a - T_o$  during DJF estimated  
870 as described in the text. The dashed line shows the time when  $T_a - T_o$  reaches the threshold  
871 that bifurcates the importance of the ENSO nonlinearity. . . . . 45
- 872 **Fig. 5.** (a): Phase diagrams showing the relationship between the cold tongue SST ( $T_2$ ) anoma-  
873 lies and the western thermocline depth departure ( $h_1$ ) anomalies simulated by the idealized  
874 model. The left (right) panel shows the one with  $T_a - T_o$  below (above) the threshold that bi-  
875 furcates the importance of the ENSO nonlinearity. The point ( $T_2', h_1'$ ) circles clockwise as the  
876 model is integrated forward in time. (b): As in (a), but for GFDL-ESM2M under RCP8.5.  
877 The western thermocline depth is defined as the depth at which the vertical temperature gra-  
878 dient reaches its maximum, and is averaged over 5°S-5°N, 140°E-150°W. After removing  
879 monthly climatology and centennial linear trends, 3-month running mean is applied. . . . . 46
- 880 **Fig. 6.** (a): As in Fig. 3 (b), but with the mean SST over the years before (colored solid) and  
881 after (colored dashed) the time when the ENSO nonlinearity becomes unimportant (black  
882 dashed). Orange (magenta) lines show the mean SST of the western warm pool (eastern  
883 cold tongue) SST. Also shown is the prescribed radiative-convective equilibrium tempera-  
884 ture (gray). (b): As in (a), but for stronger green house forcing with  $T_a - T_o$  kept the same  
885 as in (a). (c): As in (a), but for observations during DJF. Also shown is the map of the  
886 annual-mean observed SST trends during 1965-2015 computed relative to the tropical Pa-  
887 cific mean trends (30°S-30°N, 90°E-60°W). Blue color denotes a warming slower than the  
888 tropical Pacific mean, not necessarily a cooling. Unit in °C/century. (d): As in (c), but for  
889 GFDL-ESM2M under RCP8.5. . . . . 47
- 890 **Fig. 7.** (a): Scatter plot showing the relationship between the ENSO nonlinearity (defined as the  
891 skewness of detrended 11-month running mean Niño3 index) and the zonal SST gradient  
892 change (defined as the centennial linear trend of Niño3 minus Niño4), calculated for GFDL-  
893 ESM2M (red, the filled marker for RCP8.5 and the circle for RCP6.0) and other 31 CMIP5

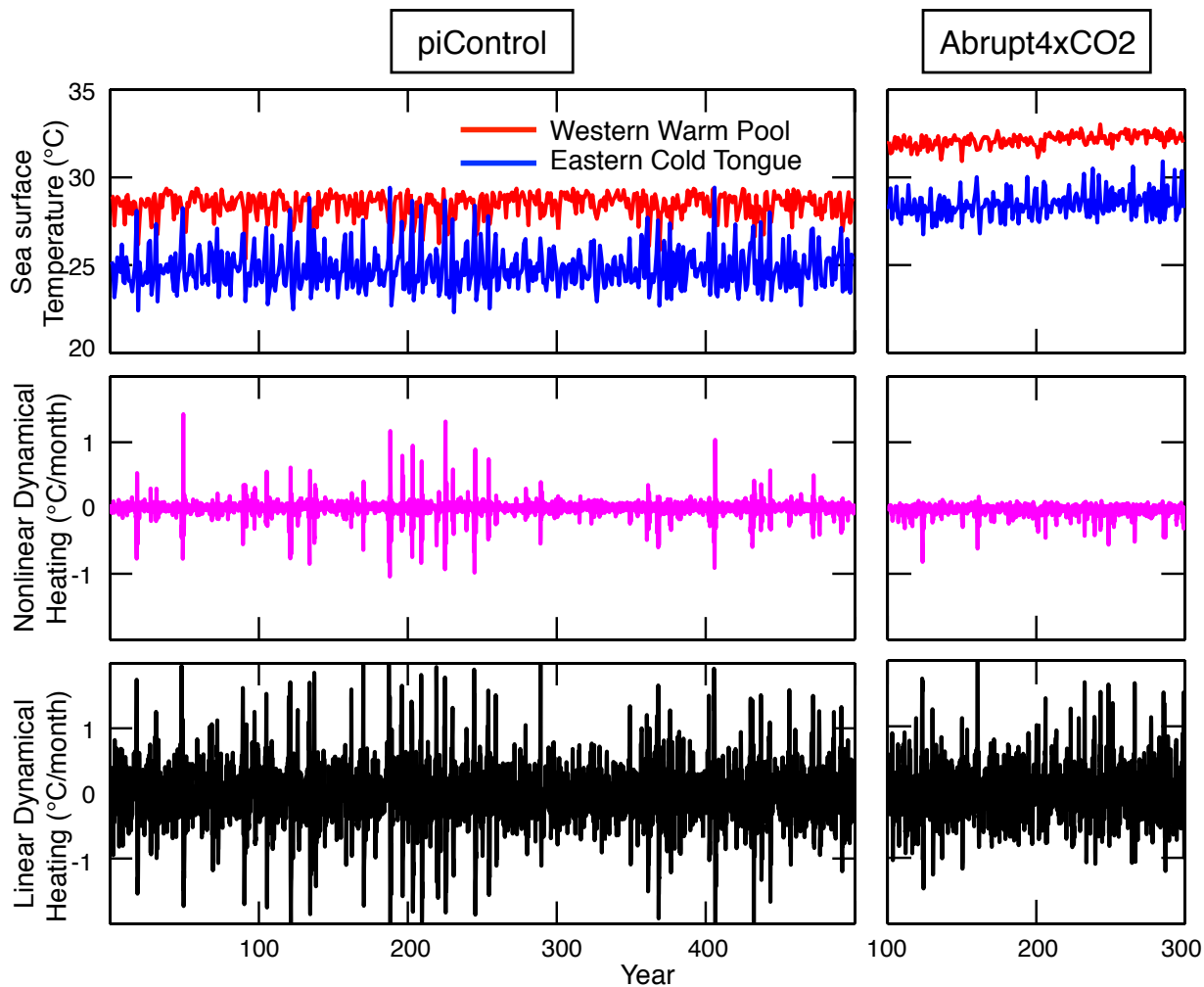
894 models (black, RCP 8.5 only). Also shown is the value for observations during 1965-2015  
895 (blue). (b): Detrended SST anomalies (SSTA) for observations, averaged over the Niño3  
896 region (5°S-5°N, 150°W-90°W). 11-month running mean is applied. (c): As in (b), but for  
897 GFDL-ESM2M under RCP8.5. (d): As in (c) but for CMIP5 models with negative or small  
898 skewness. (e): As in (d), but with few extreme El Niño events. (f): As in (d), but with  
899 excessive extreme El Niño events. . . . . 48

900 **Fig. 8.** (a): As in the bottom panel in Fig. 6 (d), but for RCP 6.0, RCP 8.5, and the first and second  
901 halves of the 1% per year increase in CO<sub>2</sub> (1pctCO<sub>2</sub>) run. (b): Left panel, Warming response  
902 calculated as difference of SST climatology in the manner of Abrupt4xCO<sub>2</sub> (Year101-300)  
903 minus piControl. Unit in °C/century. Right panel, As in (a), but for Abrupt4xCO<sub>2</sub> (Year1-  
904 300). . . . . 49

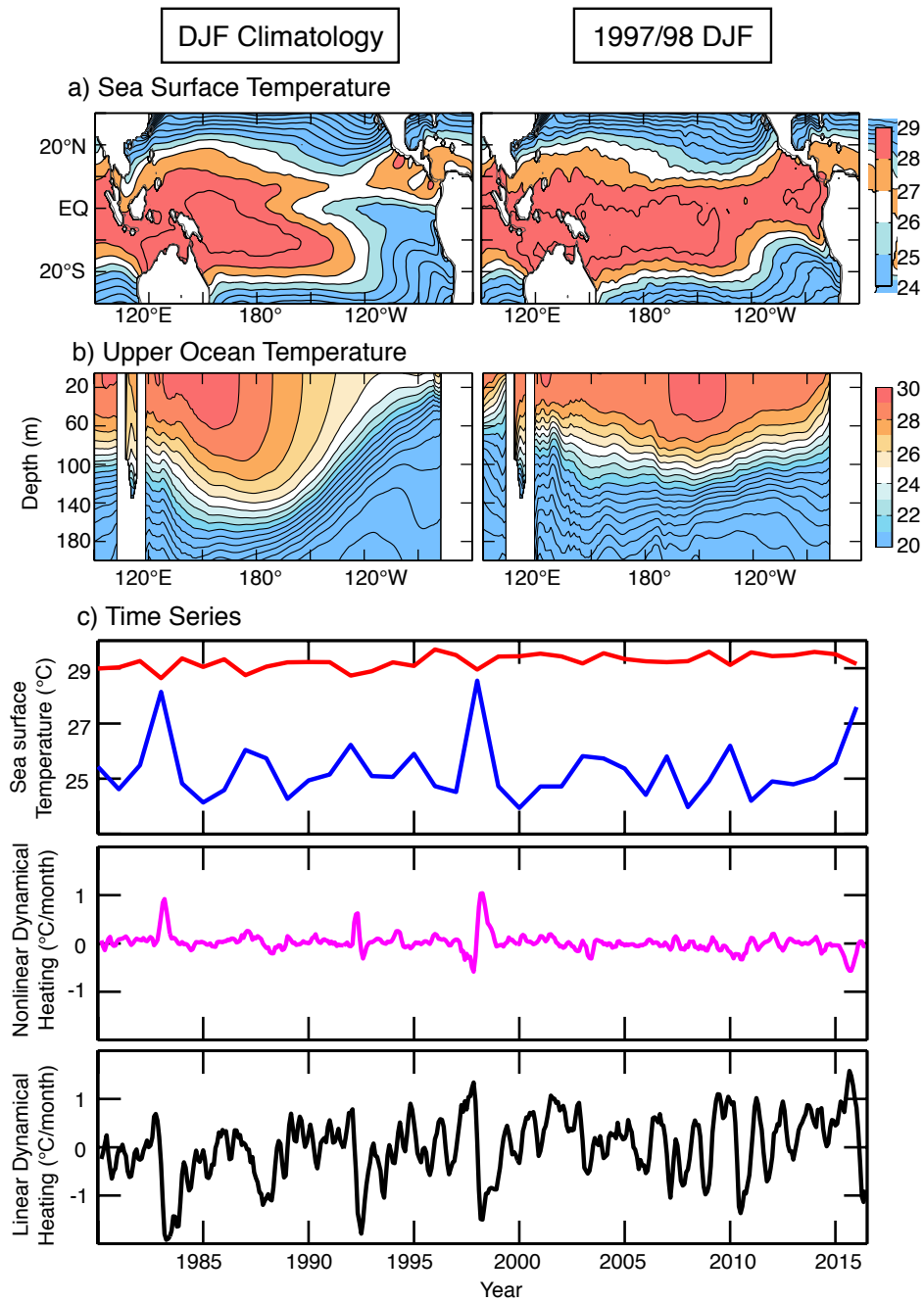
905 **Fig. 9.** (a): Flow chart showing the scenario where the Nonlinear ENSO Warming Suppression  
906 (NEWS) mechanism works, which appears to be realized only by GFDL-ESM2M with a  
907 gradual increase of CO<sub>2</sub>. (b): As in (a), but without NEWS. The majority of the CMIP5  
908 models follows this scenario. (c): As in (a), but for an abrupt warming scenario. . . . . 50

909 **Fig. 10.** (a): As in Fig. 3 (a), but the atmospheric reservoir is not fixed to the radiative-convective  
910 equilibrium temperature. Also shown at the bottom is  $T_a - T_o$ . (b): Top and Middle panels,  
911 As in (a), but for GFDL-ESM2M under piControl (Year211-305, DJF). 15-year running  
912 mean is applied to  $T_a - T_o$ . Bottom panel, As in the bottom panel of Fig. 6 (d), but for  
913 piControl (Year211-305). (c): As in (b), but for Year306-400. . . . . 51

914 **Fig. 11.** (a): Atmospheric reservoir temperature simulated by the idealized model with zero at-  
915 mospheric sensitivity to the cold tongue SST (navy blue). Also shown is the prescribed  
916 radiative-convective equilibrium temperature (gray). (b): Top panel, As in (a), but for non-  
917 zero atmospheric sensitivity to the cold tongue SST. Also shown are the periods of global  
918 warming hiatuses (green). Middle and Bottom panels, As in Fig 10 (a), but increasing the  
919 radiative-convective equilibrium temperature and oceanic reservoir temperature. (c): As in  
920 the top and bottom panels of (b), but for observations. Atmospheric reservoir temperature  
921 is replaced by annual-mean, global-mean surface temperature relative to the base period of  
922 1951-1980. SST is averaged over DJF. . . . . 52

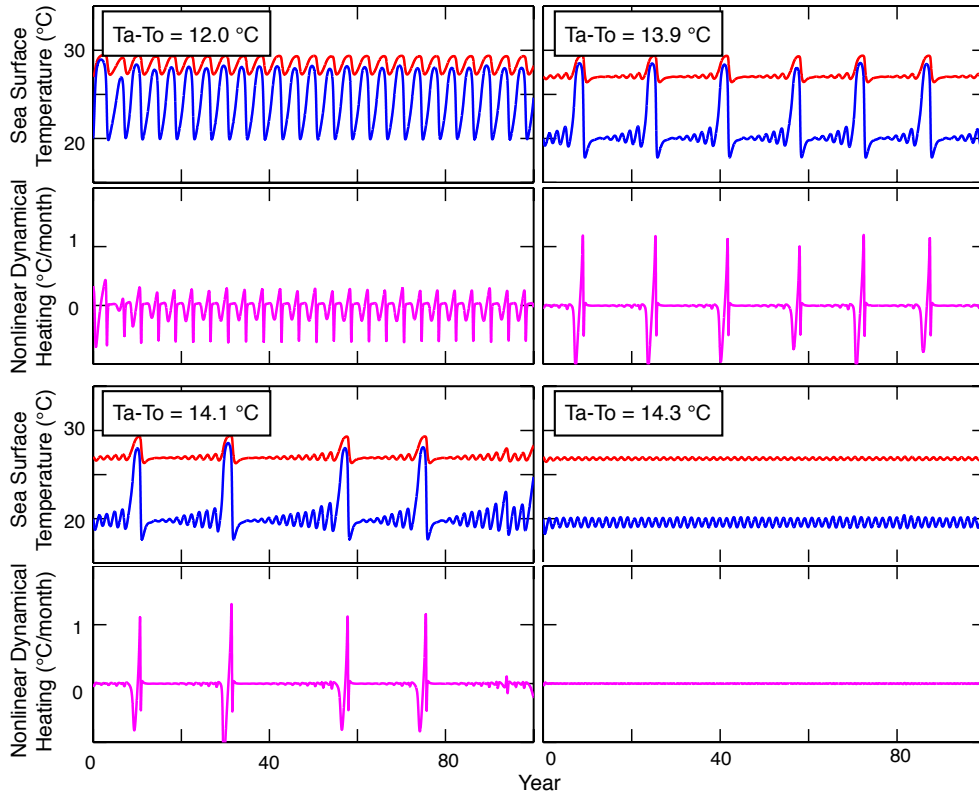


923 FIG. 1. Top panel, Sea surface temperature (SST) averaged over December-January-February (DJF), sim-  
 924 ulated by GFDL-ESM2M under the preindustrial control (piControl) and abrupt quadrupling carbon dioxide  
 925 (Abrupt4xCO<sub>2</sub>) scenarios. Red curves show the SST time series averaged over the western warm pool (5°S-  
 926 5°N, 130°E-160°E), and the blue curves show those of the eastern cold tongue (5°S-5°N, 120°W-90°W). For  
 927 Abrupt4xCO<sub>2</sub>, only after Year100 is shown because it takes several decades before the system reaches its quasi-  
 928 equilibrium. Middle and Bottom panels, Nonlinear Dynamical Heating (NDH; middle) and Linear Dynamical  
 929 Heating (LDH; bottom) time series calculated using equation (1) for the same model runs as in the top panel,  
 930 averaged over 5°S-5°N, 170°W-100°W. 3-month running mean is applied to both time series.

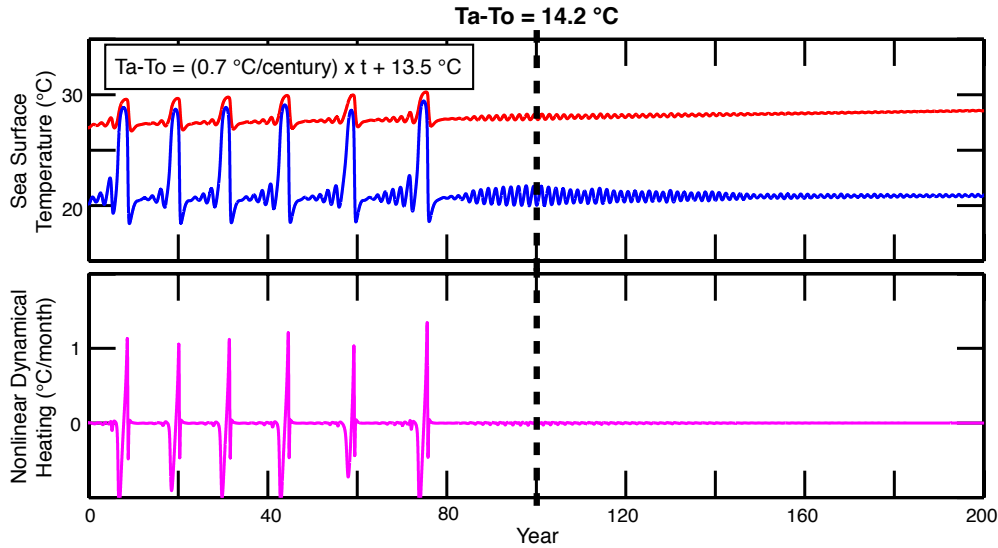


931 FIG. 2. (a): Left panel, Observed SST climatology during December-January-February (DJF). Contour inter-  
 932 val is 1°C. Right panel, As in left, but for 1997/98 DJF. (b): As in (a), but for observed upper ocean potential  
 933 temperature. (c): As in Fig. 1, but for observations.

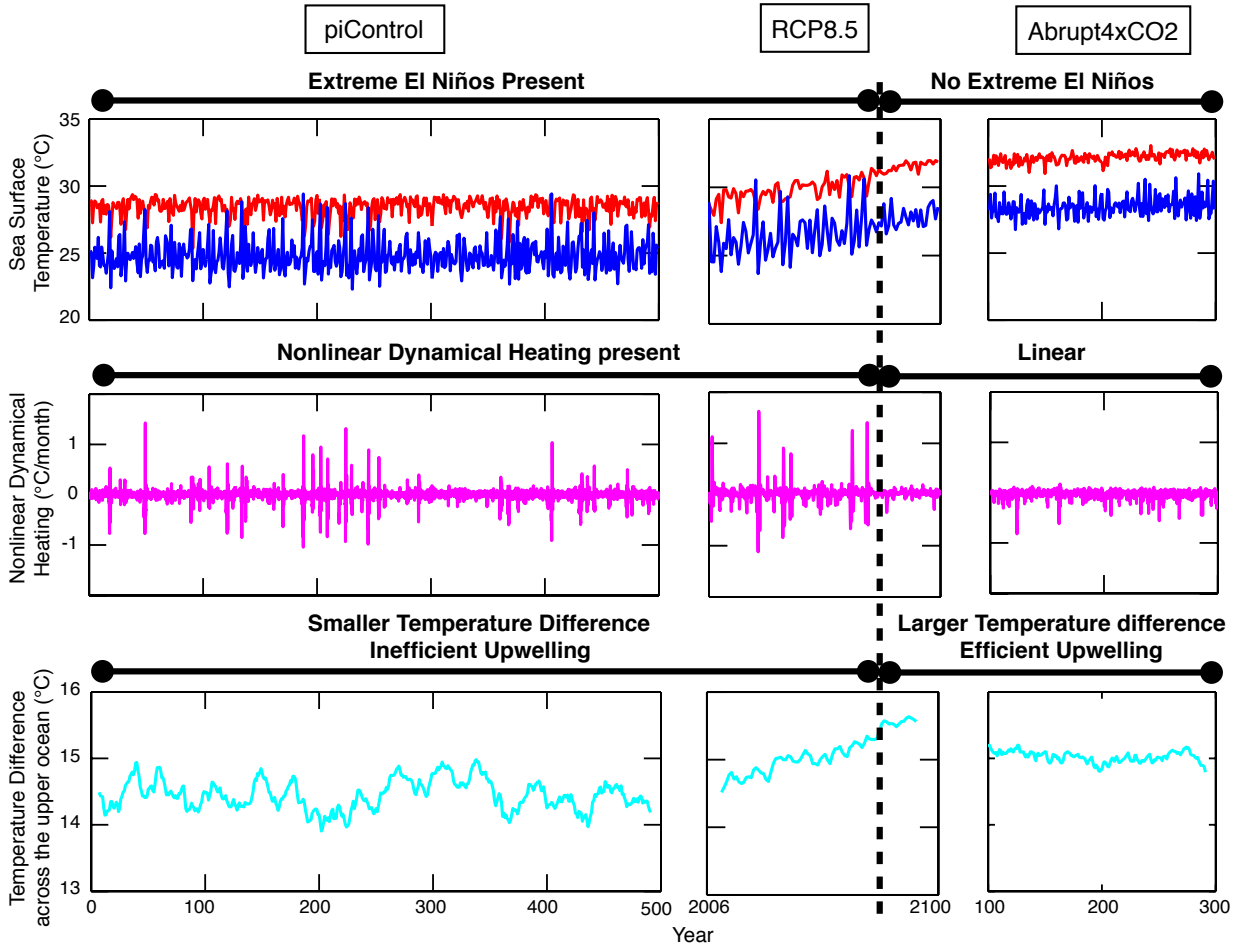
a) Fixed reservoir temperature difference



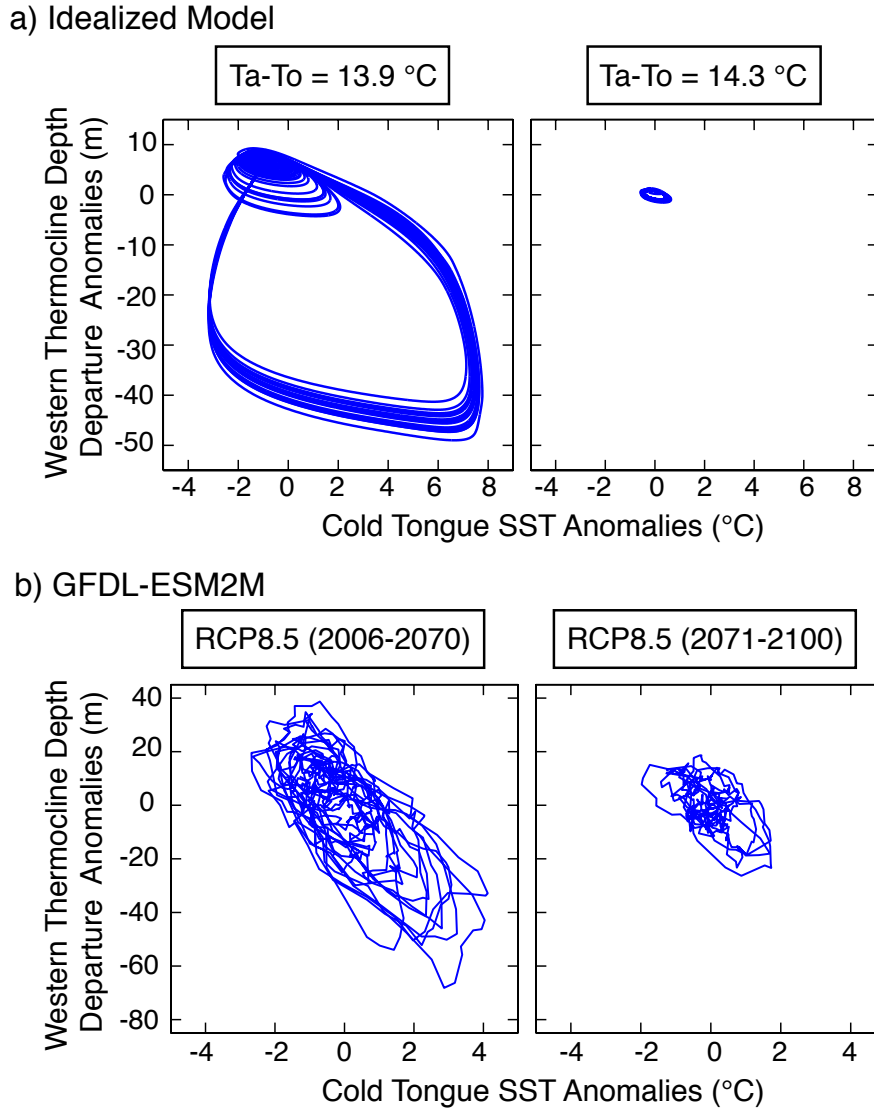
b) Increasing reservoir temperature difference



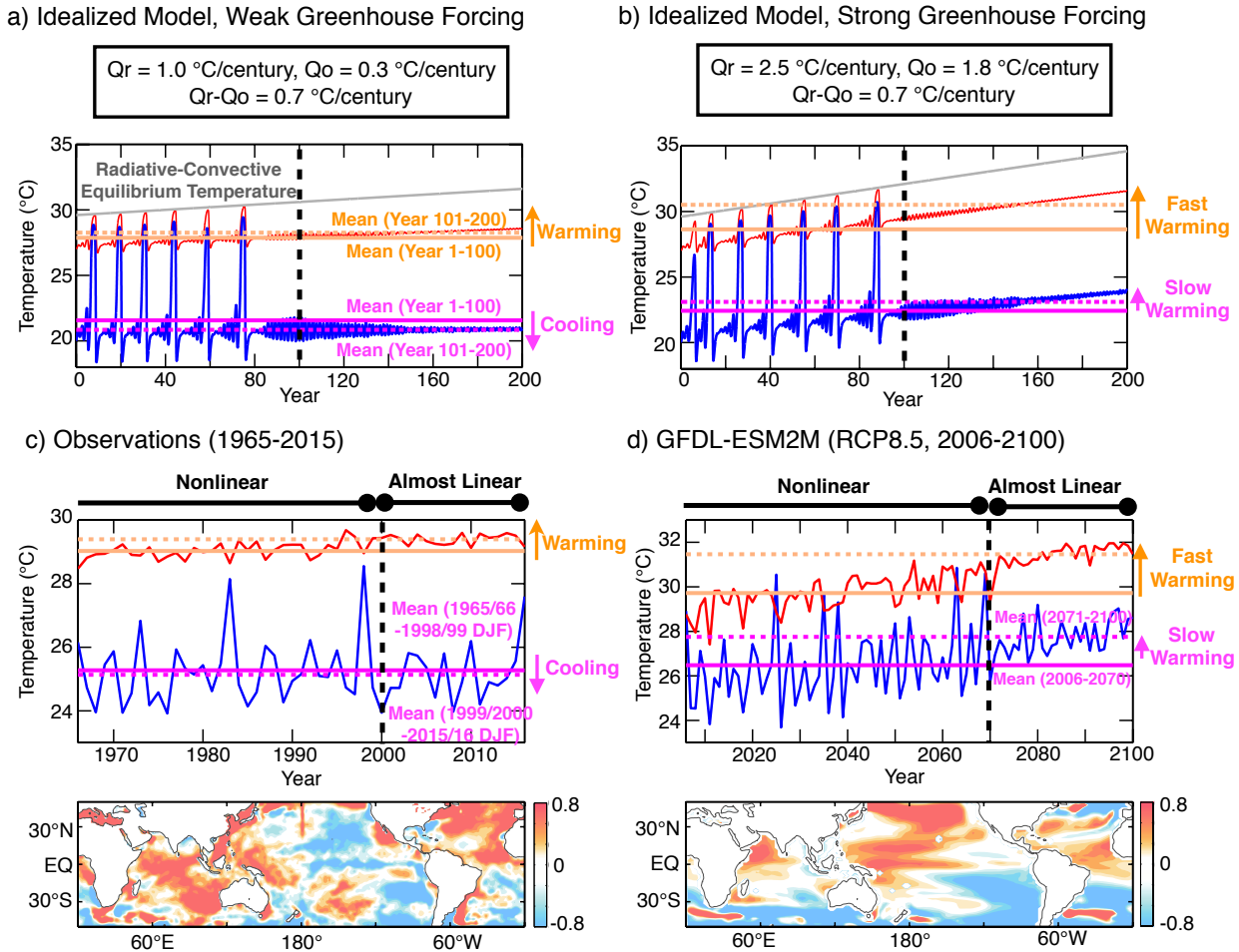
934 FIG. 3. (a): As in the top and middle panels in Fig. 1, but for the idealized model. Each panel shows a  
 935 simulation with fixed temperature difference between the atmospheric and oceanic reservoir ( $T_a - T_o$ ) indicated  
 936 at the top left. (b): As in (a), but increasing  $T_a - T_o$  following the equation shown at the top left. The dashed line  
 937 shows the time when  $T_a - T_o$  reaches the threshold that bifurcates the importance of the ENSO nonlinearity.



938 FIG. 4. As in the top and middle panels of Fig. 1, but panels for RCP 8.5 scenario is inserted between  
 939 piControl and Abrupt4xCO<sub>2</sub>. The scale of the horizontal axes for RCP 8.5 is expanded by a factor of 2. Also  
 940 shown at the bottom is 15-year running mean  $T_a - T_o$  during DJF estimated as described in the text. The dashed  
 941 line shows the time when  $T_a - T_o$  reaches the threshold that bifurcates the importance of the ENSO nonlinearity.

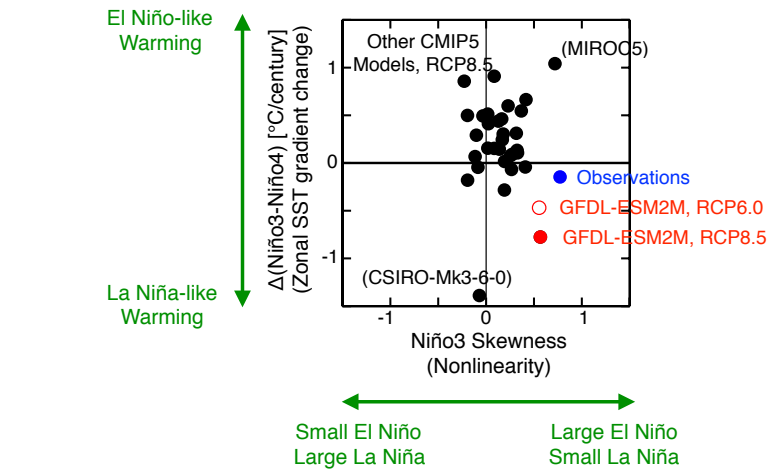


942 FIG. 5. (a): Phase diagrams showing the relationship between the cold tongue SST ( $T_2$ ) anomalies and the  
 943 western thermocline depth departure ( $h_1$ ) anomalies simulated by the idealized model. The left (right) panel  
 944 shows the one with  $T_a - T_o$  below (above) the threshold that bifurcates the importance of the ENSO nonlin-  
 945 earity. The point  $(T_2', h_1')$  circles clockwise as the model is integrated forward in time. (b): As in (a), but for  
 946 GFDL-ESM2M under RCP8.5. The western thermocline depth is defined as the depth at which the vertical tem-  
 947 perature gradient reaches its maximum, and is averaged over  $5^\circ\text{S}-5^\circ\text{N}$ ,  $140^\circ\text{E}-150^\circ\text{W}$ . After removing monthly  
 948 climatology and centennial linear trends, 3-month running mean is applied.

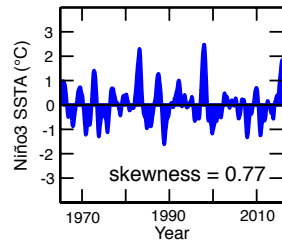


949 FIG. 6. (a): As in Fig. 3 (b), but with the mean SST over the years before (colored solid) and after (colored  
 950 dashed) the time when the ENSO nonlinearity becomes unimportant (black dashed). Orange (magenta) lines  
 951 show the mean SST of the western warm pool (eastern cold tongue) SST. Also shown is the prescribed radiative-  
 952 convective equilibrium temperature (gray). (b): As in (a), but for stronger green house forcing with  $T_a - T_o$  kept  
 953 the same as in (a). (c): As in (a), but for observations during DJF. Also shown is the map of the annual-mean  
 954 observed SST trends during 1965-2015 computed relative to the tropical Pacific mean trends (30°S-30°N, 90°E-  
 955 60°W). Blue color denotes a warming slower than the tropical Pacific mean, not necessarily a cooling. Unit in  
 956 °C/century. (d): As in (c), but for GFDL-ESM2M under RCP8.5.

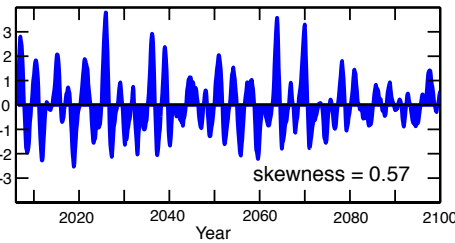
a) Zonal SST gradient change and Nonlinearity of the CMIP5 models



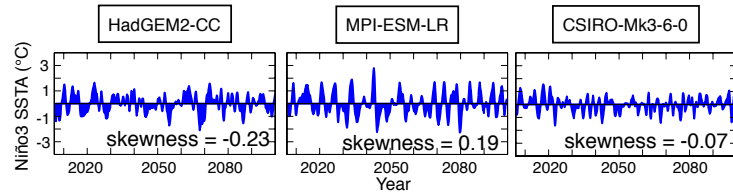
b) Observations



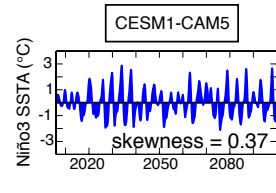
c) GFDL-ESM2M



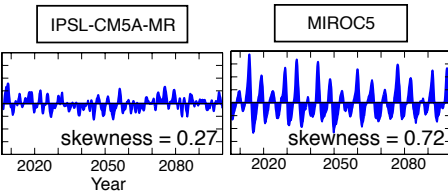
d) Opposite / Insufficient asymmetry



e) Few extreme El Niños

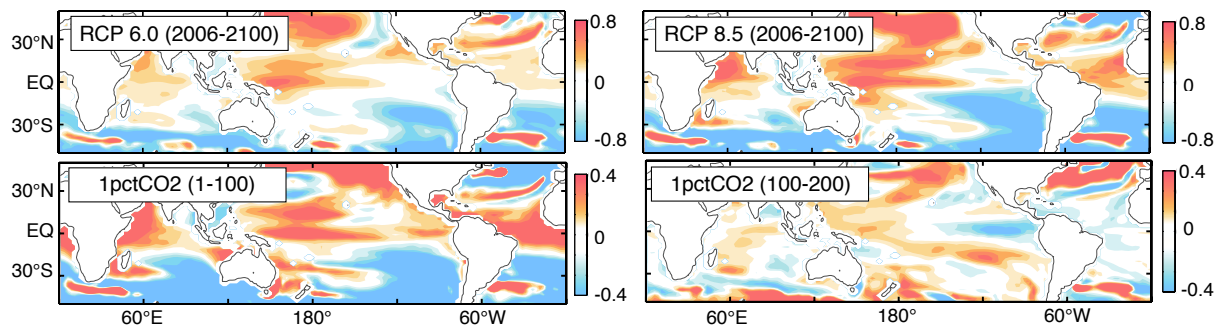


f) Excessive extreme El Niños

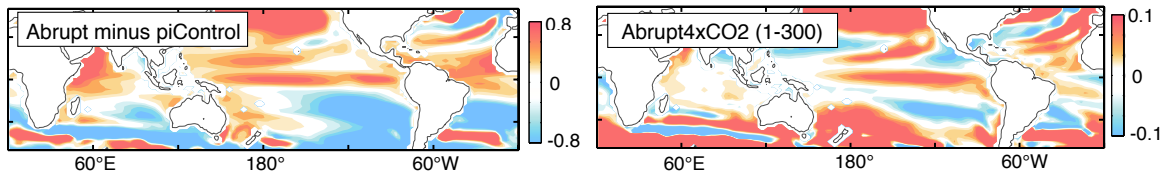


957 FIG. 7. (a): Scatter plot showing the relationship between the ENSO nonlinearity (defined as the skewness of  
 958 detrended 11-month running mean Niño3 index) and the zonal SST gradient change (defined as the centennial  
 959 linear trend of Niño3 minus Niño4), calculated for GFDL-ESM2M (red, the filled marker for RCP8.5 and the  
 960 circle for RCP6.0) and other 31 CMIP5 models (black, RCP 8.5 only). Also shown is the value for observations  
 961 during 1965-2015 (blue). (b): Detrended SST anomalies (SSTA) for observations, averaged over the Niño3  
 962 region (5°S-5°N, 150°W-90°W). 11-month running mean is applied. (c): As in (b), but for GFDL-ESM2M  
 963 under RCP8.5. (d): As in (c) but for CMIP5 models with negative or small skewness. (e): As in (d), but with  
 964 few extreme El Niño events. (f): As in (d), but with excessive extreme El Niño events.

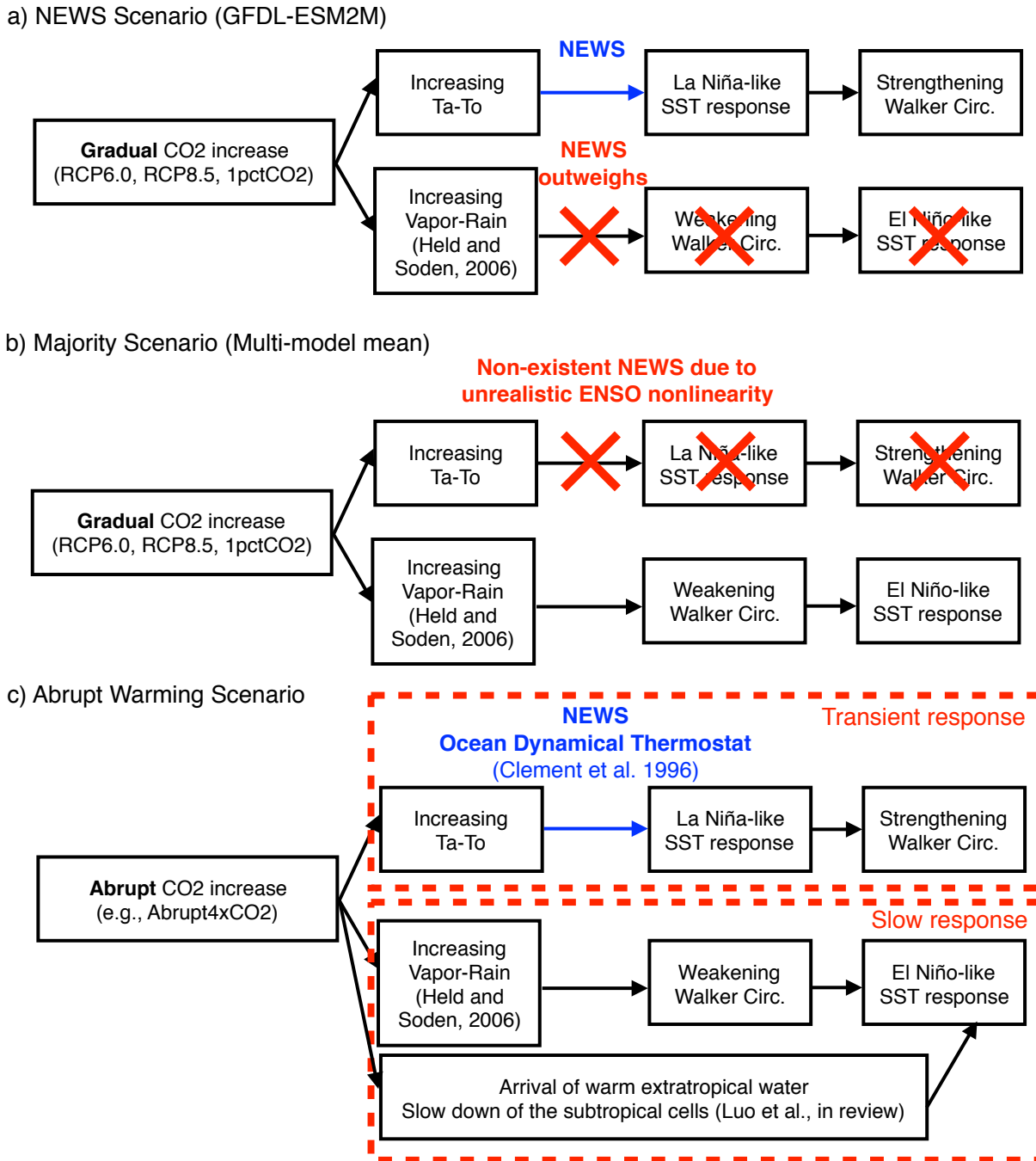
a) Gradual CO<sub>2</sub> Increase



b) Abrupt CO<sub>2</sub> Increase

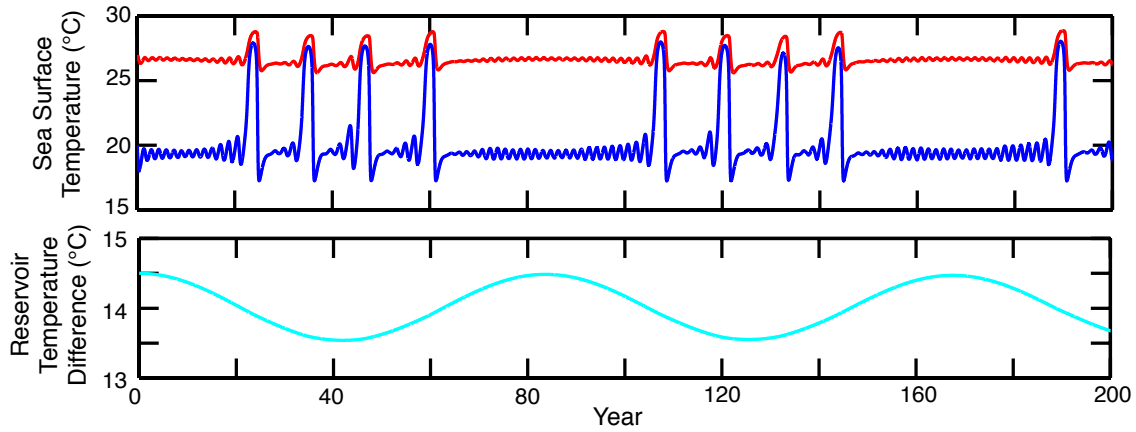


965 FIG. 8. (a): As in the bottom panel in Fig. 6 (d), but for RCP 6.0, RCP 8.5, and the first and second halves  
 966 of the 1% per year increase in CO<sub>2</sub> (1pctCO<sub>2</sub>) run. (b): Left panel, Warming response calculated as difference  
 967 of SST climatology in the manner of Abrupt4xCO<sub>2</sub> (Year101-300) minus piControl. Unit in °C/century. Right  
 968 panel, As in (a), but for Abrupt4xCO<sub>2</sub> (Year1-300).



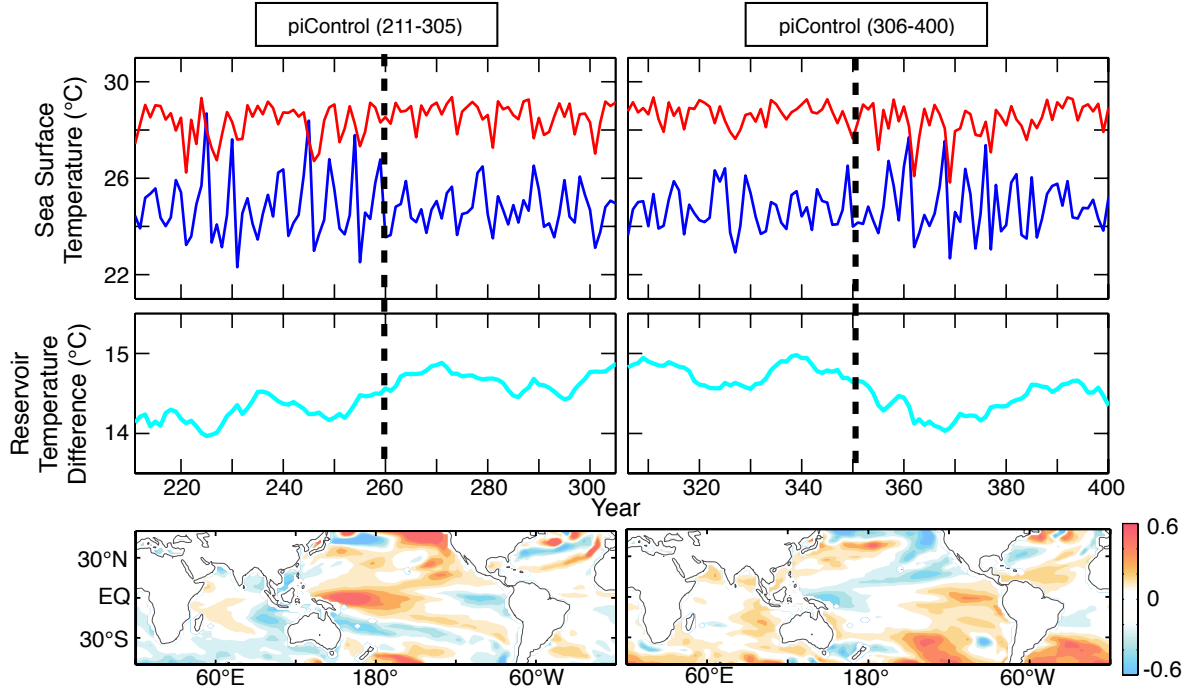
969 FIG. 9. (a): Flow chart showing the scenario where the Nonlinear ENSO Warming Suppression (NEWS)  
 970 mechanism works, which appears to be realized only by GFDL-ESM2M with a gradual increase of CO<sub>2</sub>. (b):  
 971 As in (a), but without NEWS. The majority of the CMIP5 models follows this scenario. (c): As in (a), but for an  
 972 abrupt warming scenario.

a) Idealized model with ocean-atmosphere interaction allowed

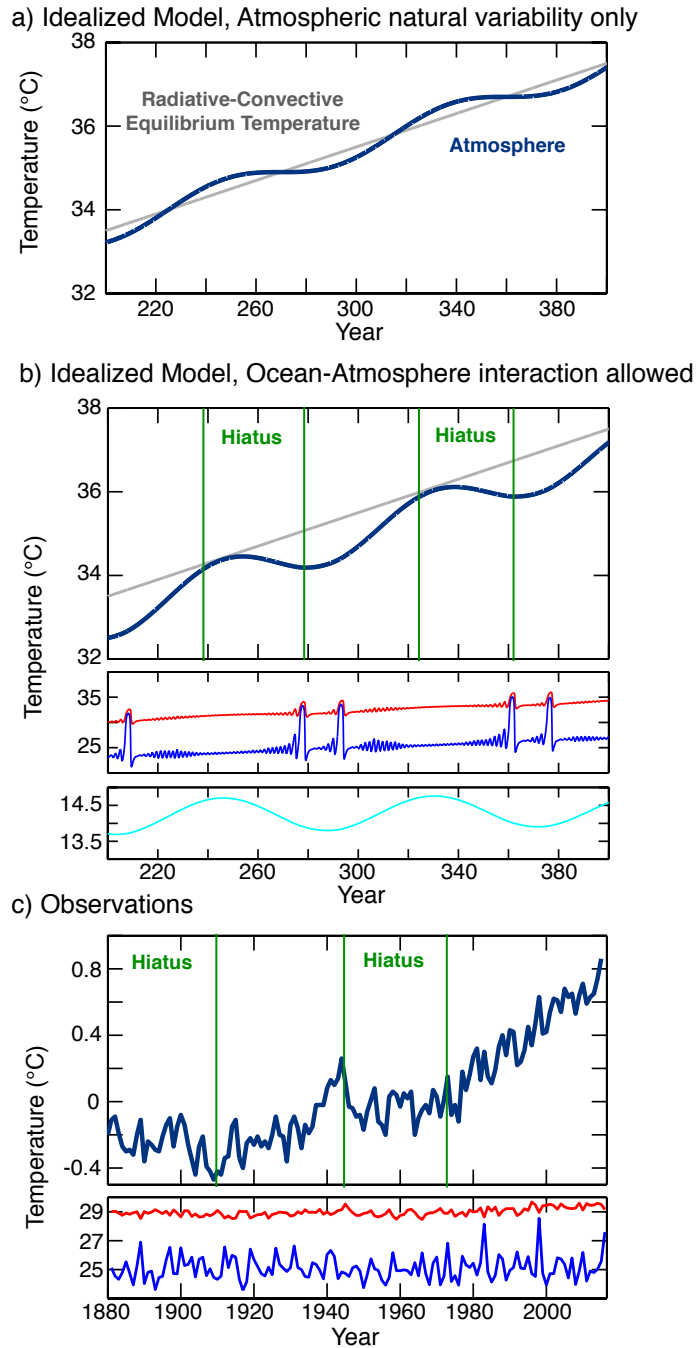


b) Nonlinear ENSO Warming Suppression (NEWS)

c) Nonlinear ENSO Warming Acceleration (NEWA)



973 FIG. 10. (a): As in Fig. 3 (a), but the atmospheric reservoir is not fixed to the radiative-convective equilibrium  
 974 temperature. Also shown at the bottom is  $T_a - T_o$ . (b): Top and Middle panels, As in (a), but for GFDL-ESM2M  
 975 under piControl (Year211-305, DJF). 15-year running mean is applied to  $T_a - T_o$ . Bottom panel, As in the bottom  
 976 panel of Fig. 6 (d), but for piControl (Year211-305). (c): As in (b), but for Year306-400.



977 FIG. 11. (a): Atmospheric reservoir temperature simulated by the idealized model with zero atmospheric  
 978 sensitivity to the cold tongue SST (navy blue). Also shown is the prescribed radiative-convective equilibrium  
 979 temperature (gray). (b): Top panel, As in (a), but for non-zero atmospheric sensitivity to the cold tongue SST.  
 980 Also shown are the periods of global warming hiatuses (green). Middle and Bottom panels, As in Fig 10 (a), but  
 981 increasing the radiative-convective equilibrium temperature and oceanic reservoir temperature. (c): As in the top  
 982 and bottom panels of (b), but for observations. Atmospheric reservoir temperature is replaced by annual-mean,  
 983 global-mean surface temperature relative to the base period of 1951-1980. SST is averaged over DJF.